Sustainable Energy & Fuels

ROYAL SOCIETY OF CHEMISTRY

REVIEW

View Article Online
View Journal | View Issue

Cite this: *Sustainable Energy Fuels*, 2022, **6**, 528

Techno-economic assessment and carbon footprint of processes for the large-scale production of oxymethylene dimethyl ethers from carbon dioxide and hydrogen†

Franz Mantei,[a] Ramy E. Ali,[a] Cornelie Baensch,[b] Simon Voelker,[c] Philipp Haltenort,[d] Jakob Burger,[e] Ralph-Uwe Dietrich,[b] Niklas von der Assen,[c] Achim Schaadt,[a] Jörg Sauer[d] and Ouda Salem *[a]

Poly(oxymethylene)dimethyl ethers (OME) show promising fuel properties, enabling their use in existing infrastructure, especially as alternatives or additives to diesel fuel, leading to a significant reduction in local emissions (*e.g.*, soot and NO_x). Additionally, OME can be produced from methanol, enabling their production based on a renewable feedstock, which can significantly reduce the carbon footprint in comparison to fossil fuels. However, an industrial process to sustainably produce OME on a large-scale has not been developed to date. Based on the results of detailed simulations in Aspen Plus®, this work compares the most promising process routes for the production of OME_{3-5} in a system boundary including H_2 *via* water electrolysis and captured CO_2 from point sources or ultimately using direct air capture technologies. One of the main outcomes of this work is the standardized methodology introduced for the techno-economic and CO_2 footprint evaluation and comparison of the diverse processes. The comparison criteria are based on systematic approaches covering process materials and energy efficiency, technology readiness level, costs, and the carbon footprint. The process routes based on anhydrous formaldehyde and methanol or methylal feedstock show higher energy efficiencies and lower carbon footprints than other routes considering the commercial aqueous formaldehyde. However, the synthesis of anhydrous formaldehyde is under research and development and not yet industrially established. Importantly, considering the net production costs of OME_{3-5} from the four simulated process routes, there is no significant difference, which is attributed to the rather high share of the operational cost, and specifically the cost of the H_2 and CO_2 feedstock. Using sensitivity analysis, the influence of feedstock costs and carbon footprint on the evaluation criteria is identified, elaborating the potential of feasible and sustainable OME production under favourable conditions.

Received 19th August 2021
Accepted 13th November 2021

DOI: 10.1039/d1se01270c

rsc.li/sustainable-energy

1. Introduction

The CO_2 emission reduction targets of the German federal government in the mobility sector were achieved in 2020 according to the German Environment Agency (UBA) report with a 19 million ton reduction to reach an overall 146 million ton of CO_2-eq. emissions. Nevertheless, this was correlated to the COVID-19 pandemic, where the mobility sector has been behind in its CO_2 emission reduction targets in the last two decades.[1] This sector is required to significantly reduce its global (mainly CO_2) and local emissions specially under the EURO 6 (NO_x < 0.08 g km^{-1}, PM < 0.0045 g km^{-1}) and the upcoming stricter EURO 7 emission reduction standards.[2] Diesel engines are currently one of the major internal combustion engines used in the mobility sector,[3,4] with their share expected to grow in various mobility sector modes (passenger vehicles, road freight, ships, *etc.*). An expected increase in oil demand by passenger vehicles from 20 million barrel per day in 2020 to 27.5 million barrel per day in 2030 was reported by the International Energy Agency (IEA) in 2020.[5] Accordingly, besides combustion engine optimization and the already complex exhaust gas system improvements, altering the

[a]*Thermochemical Processes Department, Division Hydrogen Technologies, Fraunhofer Institute for Solar Energy Systems, Heidenhofstr. 2, 79110, Freiburg, Germany. E-mail: ouda.salem@ise.fraunhofer.de*

[b]*Energy System Integration, Institute of Engineering Thermodynamics, German Aerospace Center, Pfaffenwaldring 38-40, 70569, Stuttgart, Germany*

[c]*Institute of Technical Thermodynamics, Energy Systems Engineering, RWTH Aachen University, Schinkelstraße 8, 52062, Aachen, Germany*

[d]*Institute of Catalysis Research and Technology, Karlsruhe Institute of Technology, Hermann-von-Helmholtz-Platz 1, 76344, Eggenstein-Leopoldshafen, Germany*

[e]*Chemical Process Engineering, Technical University of Munich, Uferstraße 53, 94315, Straubing, Germany*

† Electronic supplementary information (ESI) available. See DOI: 10.1039/d1se01270c

active combustion substance (fuel) is one of the most effective strategies to achieve these emission reduction targets.

Poly(oxymethylene)dimethyl ethers with the chemical formula $H_3C–(O–CH_2)_n–O–CH_3$ where $n \geq 2$ (denoted hereon as OME) can be blended with diesel fuel or applied as neat fuel in diesel combustion engines, resulting in significant reductions in local emission (*i.e.*, soot and NO_x). This is due to the chemical structure of OME, which has no direct C–C bond, their high intermolecular oxygen content and favourable fuel properties. This also enables the use of existing infrastructure for the transportation, storage, and distribution of OME blends with diesel.[6–9] The well-to-wheel (WtW) CO_2 emissions can be significantly reduced compared to fossil-based fuels if OME are produced from renewable carbon sources and low-carbon H_2.[10] Several studies investigated different blends of OME with diesel fuel to conform to the EN590 standard, which showed a significant reduction in local emissions for both heavy duty and passenger cars.[11–24] Under certain conditions, even a mixture of 10 vol% OME with diesel can lead to a significant reduction in NO_x and soot emissions.[12] A stoichiometric evaluation showed that already 10 vol% OME blend with diesel will correspond to *ca.* 441 billion litres (diesel equivalent) per year OME production capacity worldwide and *ca.* 7.58 billion litres per year for Germany, which emphasizes the need for large-scale production plants in blending cases. Various blending rates were investigated in heavy duty and passenger car engines by several researchers, showing significant potential to increase the engine efficiency by increasing the exhaust gas recirculation (EGR) as a consequence of overcoming NO_x and soot trade-off.[25–27]

Importantly, life cycle assessment (LCA) studies showed the potential of CO_2 reduction based on neat OME or blends with fossil or Fischer–Tropsch diesel. For a certain case study using neat $OME_{3–5}$, Hank *et al.* evaluated that the WtW greenhouse gas emissions (GHGE) can be reduced by 86%, corresponding to 29 g(CO_2-eq.) km^{-1} ($OME_{3–5}$-fuel) compared to 209 g(CO_2-eq.) km^{-1} (diesel fuel).[10] Deutz *et al.* investigated the WtW LCA for methylal (OME_1) and concluded that it has the potential to serve as an almost carbon-neutral blending component, where replacing 24 wt% diesel with OME_1 could reduce the global warming impact by 22% and the emissions of NO_x and soot by 43% and 75%, respectively.[28] However, special sealing materials such as ethylene propylene diene rubber (EPDM)[26,29] and fuel injection system modifications are needed to achieve certain blending rates of OME with diesel fuel.[9] Neat OME applications are discussed using dedicated engines for niche markets (*e.g.*, agricultural engines, stationary engines, and hand-used machinery) and for captive fleets (public buses, trains, *etc.*).[30,31]

Moreover, a recent study by Frontier Economics[32] concluded that Power-to-X (PtX) fueled internal combustion engine vehicles (ICEVs) possess advantages over battery electrical vehicles (BEVs) considering the complete value chain efficiency and importantly; including the renewable generator yield efficiency and the fluctuating nature of renewable electricity production. The study concluded that the overall efficiency factor in a holistic consideration between BEVs and ICEVs is between 1.1 and 1.6. Considering that PtX synthetic fuels can be produced wherever there is high renewable energy (RE) resource penetration and dense fuels can be easily imported to the utilization point, PtX fuels can be added to existing infrastructure, offering an efficient, fast and reliable solution. Particularly, for transport modes that indeed require high density fuels (aviation, ships, trucks, *etc.*), there are no feasible means to achieve defossilization targets without PtX fuels.

OME production processes have been investigated intensively since the early work by DuPont in the middle of the 20th century on the production of longer chain OME.[33] Since the 1990s, short chain OME have been recognized as interesting diesel blends or substitutes.[34] Subsequently, intensive research efforts have been focused on engine testing on one hand, and production processes on the other hand, led by Ford motor company and Eni SpA.[35,36] At the beginning of the 21st century, fundamental developments led by BASF and BP established the production processes for OME on research and pilot scales. Most of the following contributions on the process side were led by Chinese research and industrial groups, especially the important work by China Petroleum & Chemical Corporation SINOPEC.[33,37] An overview of the publications and the patents, together with the research activities in Germany and worldwide considering OME is given in the review work by Hackbarth *et al.*,[38] elaborating the intensity of research in this field. Currently, some OME plants are in operation or under construction as reported in China with production capacities of 10–400 kt per annum mostly based on the commercial fossil-based feedstock OME_1 or methanol and paraformaldehyde (pFA) or formalin.[38] The product quality, reproducibility, and long-term production capacities of these plants are not defined due to their varying operational strategies. Additionally, the complexity of these plants to achieve pure OME products could limits the scalability of these technologies to the desired large-scale, which is needed in the context of usage as a fuel.

Considering the value chain starting from H_2 and CO_2 towards OME production or partially considering the production of OME based on the feedstock methanol, several techno-economic assessments (TEA) and process simulations for different synthetic routes were pursued. The studies highlighted insights regarding the economic potential of OME production and hurdles regarding the demonstration and technology realization. Prominently, the work by Burger *et al.*,[39] Schemme *et al.*,[40] Bongartz *et al.*,[41] Ouda *et al.*,[42] and Held *et al.*[43] were considered. However, the underlying assumptions, considered process routes, scope of the evaluation, modelling approaches and boundary conditions vary among these contributions, which lead to different conclusions and complicates the comparison between different process routes. Additionally, a complete and detailed process description identifying the material and energy integration concepts of the sub-processes in a complete process chain, where engineering data and TEA data can be extracted are lacking. The purification of a highly non-ideal and reactive product mixture containing several heterogeneous azeotropes, complex vapor–liquid–liquid equilibria (VLLE), especially the separation of water and formaldehyde from the target OME product, and challenges regarding solidification are cumbersome. This leads to simplification strategies and assumptions, particularly on the product purification side, which in some

cases lead to misleading results concerning the OME product composition and purity. Additionally, material and energy balances can deviate significantly from experimental cases.

In the light of the previous discussion, the introduction of OME to the market at large-scale requires next to the technological developments, a detailed comparison and evaluation of material and energy integrated, efficient, economically feasible and scalable industrial process routes for the production of OME with a certain chain length.

Objectives

Herein, as part of the project Sustainable Mobility through Synthetic Fuels (NAMOSYN), the most promising OME production process routes are evaluated using a standardized simulation methodology with the objective to evaluate and compare the promising process routes and obtain the design parameters for the first European large-scale OME production process.

In addition to the OME production process concepts, the validation of the employed models using numerous published experimental data will be described. Furthermore, based on the modelling results, the material and energy integrated process, energy efficiency, carbon footprint and the TRL of the investigated process routes will be introduced and discussed. Correspondingly, the net production costs of OME will be presented together with a sensitivity analysis covering the cost impact for H_2 and CO_2, showing the potential for the sustainable production of OME_{3-5}. Finally, the understanding from this work can highlight the critical process components in the OME value chain for further R&D endeavours.

2. Theory and background

For the synthesis of OME, methyl-capping groups such as methanol (H_3C–OH, MeOH), methylal (H_3C–O–$(CH_2O)_1$–CH_3, OME_1), and dimethyl ether (H_3C–O–CH_3, DME) need to react over acid catalysts with a source of formaldehyde group such as formalin, paraformaldehyde (HO–$(CH_2O)_n$–H with n = 8–100, pFA), trioxane ($C_3H_6O_3$, TRI), and anhydrous formaldehyde (H_2C–O, FA). The reaction proceeds through an initiation, growth, and termination mechanism, as described by Baranowski *et al.*,[44] Schmitz *et al.*,[45–48] and Oestreich *et al.*[49] This leads to several simultaneous catalyzed and non-catalyzed reactions and the formation of undesirable side-products such as poly-(oxymethylene)hemiformals (HF), poly-(oxymethylene) glycols (MG), water, and others, as shown in Fig. 1 and extended in the ESI.† The formation of the unstable HF and MG was experimentally investigated and quantified using NMR techniques in a series of fundamental studies, mainly by the group of Hasse *et al.*,[50–53] where the concepts of the "overall composition" and the "true composition" were introduced. The "true composition" is not measurable using standard analytical techniques and represents all the reaction mixture components, namely, MeOH, H_2O, FA, OME_{1-n}, HF_n, MG_n and possible side products. The "overall composition" represents the decomposition of HF and MG to their original reactants of MeOH, H_2O and FA. This is a deciding aspect in process modelling and simulation,

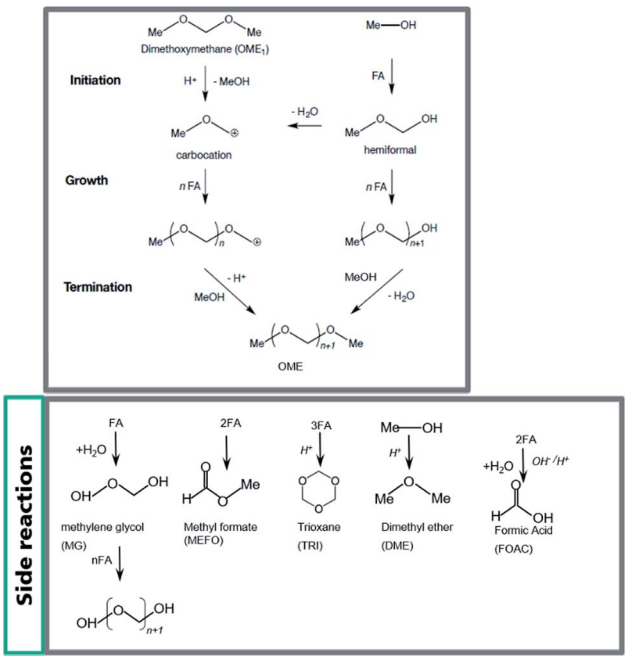

Fig. 1 Reaction network and mechanism of OME formation based on different methyl-capping groups and formaldehyde, inspired by ref. 44.

especially considering reaction and separation process design.[45–48] Estimations of heating and cooling duties, power loads and size of unit operation depend on thermodynamic and physical properties of the pure components such as heat capacity, enthalpy of vaporization and vapor pressure to account for real phase behaviour and phase equilibria. Therefore, these results are influenced significantly by the true or the overall composition. Besides, to date, components such as OME, HF and MG are not included in commercial flowsheet simulation software. The thermodynamic properties of these intermediates are described in the original literature but the right property implementation and consideration in a process simulation require fundamental knowhow about this reactive system. The work by Maurer, Hasse, Burger and Schmitz *et al.*[45–48,54] offers a concrete basis for the validation of the simulation models. Furthermore, the methodology of the implementation of these reaction and phase behaviour considerations along with the whole flowsheet simulation was introduced by Bongartz *et al.*[41] employing tool boxes from the electrochemical field, namely, the chemistry section in ASPEN Plus® and is further modified in this work. There have been several significant modelling and simulation efforts to describe this complex system behaviour, where the works by Burger *et al.*,[39] Schmitz *et al.*,[45–48] Bongartz *et al.*,[41] and Ouda *et al.*[42] are acknowledged, and the simulation results generated in this work are a progression on their previous work.

3. Process description

As described previously, OME can be produced starting from different feedstocks. Based on this, several process routes can be allocated to produce a desired mixture of OME_{3-5}. An

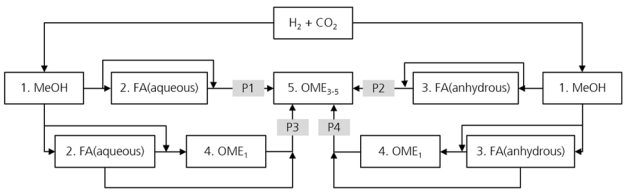

Fig. 2 Evaluated process routes towards OME_{3-5}.

overview of the four selected promising process routes investigated in this work is shown in Fig. 2. The selection of the processes focuses on the feedstock availability on a large-scale, technological maturity of the considered processes and availability of experimental data for consistent process evaluation.

All four process routes (denoted here as P1–P4) start with the synthesis and purification of MeOH from the H_2 and CO_2 feedstocks. MeOH is converted into intermediate products, namely, FA and OME_1, which are further used to synthesize a mixture containing OME_n with $n = 1$–10. This mixture is then fractionated to obtain a final product mixture containing OME_{3-5}. Consequently, the conversion of MeOH to OME_{3-5} goes through different subprocesses, which in turn influence the total process energy efficiency and the product yields. These subprocesses are MeOH synthesis, FA (aqueous) synthesis, FA (anhydrous) synthesis, OME_1 synthesis and OME_n synthesis. The combinations thereof lead to the aforementioned production routes of OME. In the following section, each of these subprocesses are briefly explained.

MeOH synthesis

MeOH synthesis is one of the oldest thermochemical processes with the highest production capacities and is mainly based on fossil feedstocks. The development of a Cu-based process enabled a significant reduction in the synthesis conditions to temperatures as low as 200–280 °C and pressure of 50–125 bar. Advanced catalyst development allows MeOH synthesis based on a CO_2-rich feed with enhanced catalyst water tolerance.[55,56] The process conditions for the synthesis of MeOH are based on the work by Otto[57] and Bongartz *et al.*[58] The reaction network considered in this work is introduced in eqn (1)–(3). The reaction equilibrium and kinetic relations are implemented based on the work by Nestler *et al.*[59] The MeOH synthesis process takes place at 250 °C and 70 bar in a plug flow reactor and the downstream purification of MeOH from non-reacted gases such as CO_2, CO, H_2 and H_2O goes through a cascade of flash drums with intermediate cooling, operating at different pressure levels, then followed by a distillation column. The light gases with the non-reactants are recycled back to the reactor to increase the product yield. A simplified flowsheet of this subprocess is shown in Fig. 3.

Main reaction network:

$$CO_2 + 3H_2 \rightleftharpoons CH_3OH + H_2O \quad (1)$$

$$CO + H_2O \rightleftharpoons CO_2 + H_2 \quad (2)$$

$$CO + 2H_2 \rightleftharpoons CH_3OH \quad (3)$$

FA (aqueous) synthesis

The FA (aqueous) subprocess comprises the conversion of MeOH to FA. Formalin or pFA is synthesized commercially from MeOH. The former is produced either *via* the silver catalyst-based process or the FORMOX process. In these processes, MeOH is partially oxidized over an Ag-based catalyst or metal oxide-based catalyst to selectively produce formalin aqueous solution (FA concentration 37–55 wt%). In the Ag-based process, MeOH is mixed with an air stream and fed to

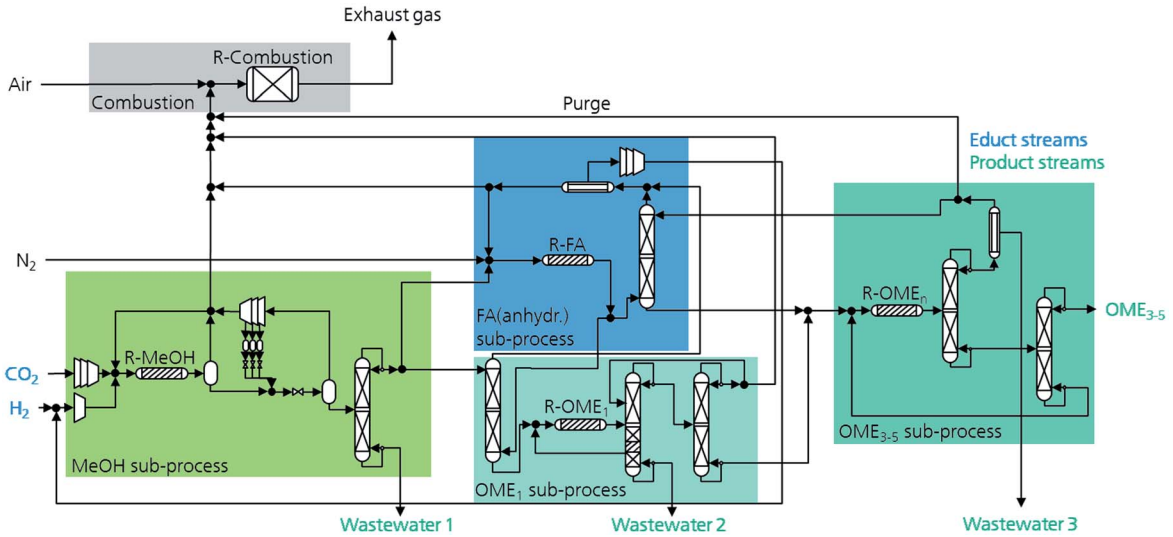

Fig. 3 Simplified process flow diagram for P4 allocation illustrating some material integration strategies and four of the five subprocesses are presented.

a reactor to be converted to FA *via* partial oxidation and dehydrogenation reactions, as shown in eqn (4)–(6).

Main reaction network:

$$CH_3OH + \tfrac{1}{2}O_2 \rightarrow CH_2O + H_2O \quad (4)$$

$$CH_3OH \rightleftharpoons CO + 2H_2 \quad (5)$$

$$CO + \tfrac{1}{2}O_2 \rightleftharpoons CO_2 \quad (6)$$

The FA (aqueous) synthesis subprocess takes place at $T > 650$ °C and near ambient pressure in a kinetically controlled regime. H_2O is formed as a by-product, and thus this subprocess is denoted heron as FA (aqueous). The process concept of this sub-process was presented by Franz *et al.*,[60] which considers the separation of FA from volatile gases in an absorber column using H_2O as a washing liquid. Providing a FA product stream containing about 55 wt% FA and 45 wt% H_2O, this stream should be concentrated to be further used for the synthesis of longer chain OMEs. Therefore, this stream is fed to a cascade of two evaporators, which split it into two output streams. The target product from this subprocess stream with about 85 wt% of FA is further used for the synthesis of longer chain OMEs, whereas the evaporator side product stream with about 10 wt% of FA is partially used as a washing liquid for the aforementioned absorber column and partially leaves the subprocess as a wastewater stream.

FA (anhydrous) synthesis

There is no commercial anhydrous FA synthesis based on the endothermic dissociation of MeOH to monomeric FA and valuable H_2 (eqn (7)), although this route has been investigated since 1960 to identify selective catalysts for the anhydrous synthesis of FA.[61] The lack of direct application of the highly reactive monomeric FA product hinders the market establishment of this production route. In the case of OME synthesis, this valuable monomeric FA product is important, and thus this subprocess is considered the "dream reaction" for the OME value chain. The reaction occurs at high temperatures > 650 °C, which requires 85 kJ mol^{-1} FA to be produced. Due to the high reactivity of FA, the retention time is very short to avoid the formation of the thermodynamically unfavoured CO, as shown in eqn (8). The challenge in this reaction system is to reach high MeOH conversions at high FA selectivity without deactivating the catalysts in this strongly reducting H_2 environment, which is an aspect that has been intensively experimentally investigated in the scientific community. For the implementation in the simulation platform, the process described by Sauer *et al.*[62] combined with the process concept published by Ouda *et al.*[42] is adapted. MeOH is saturated in a carrier gas and further dissociated at 900 °C to FA and H_2 over an Na-based catalyst, following the complete MeOH conversion and selectivity experimentally investigated by Sauer *et al.*[62] CO is formed as an undesired side-product. For the separation of the monomeric FA from the reaction products, absorber columns using mainly MeOH or recycled OME fractions as washing liquids are used.

Main reaction network:

$$CH_3OH \rightleftharpoons CH_2O + H_2 \quad (7)$$

$$CH_3OH \rightleftharpoons CO + 2H_2 \quad (8)$$

OME_1 synthesis

Methylal is available commercially based on MeOH and FA feedstock. The OME_1 subprocess comprises the conversion of MeOH and FA to OME_1. For the implementation of this subprocess, the process concept was adapted from Drunsel.[63] The synthesis takes place *via* a heterogenous catalytic reaction at 60 °C and 2 bar over an acidic catalyst, *e.g.*, Amberlyst® 15, in a plug flow reactor. Several reactions are possible, as shown in the reaction network eqn (9)–(13). The reaction product purification takes place in a downstream reactive distillation column. The column is used to overcome the reaction equilibrium restrictions and convert the rest of FA almost completely to OME_1, while separating H_2O and MeOH from the azeotropic mixture of OME_1 and MeOH. In a consecutive distillation column operating at a higher-pressure level, OME_1 is separated from the azeotropic mixture of OME_1 and MeOH and leaves the distillation column as the bottom product. The distillate product is recycled to the reactive distillation column.

Main reaction network:

$$CH_2O + H_2O \rightleftharpoons HO(CH_2O)_1H \quad (9)$$

$$CH_2O + HO(CH_2O)_{n-1}H \rightleftharpoons HO(CH_2O)_nH;\ n \geq 2 \quad (10)$$

$$CH_2O + CH_3OH \rightleftharpoons HO(CH_2O)_1CH_3 \quad (11)$$

$$CH_2O + HO(CH_2O)_{n-1}CH_3 \rightleftharpoons HO(CH_2O)nCH_3;\ n \geq 2 \quad (12)$$

$$HO(CH_2O)_1CH_3 + CH_3OH \overset{H^+}{\rightleftharpoons} CH_3O(CH_2O)_1CH_3 + H_2O \quad (13)$$

Higher OME synthesis and purification

For the implementation in the simulation platform, the higher OME subprocess comprises the conversion of the aforementioned intermediates selectively to longer-chain OME and the purification of the target OME_{3-5} product. The process concept adapted here is suitable for different feedstocks and was proposed by Schmitz *et al.*[39,46] OME_n synthesis takes place *via* a heterogenous catalytic reaction at 80 °C and 2 bar in a plug flow reactor in the presence of an acidic catalyst, *e.g.*, Amberlyst® 46. The reaction network taking place here is presented in eqn (9)–(15) and summarized in Fig. 1. The reaction product purification takes place in a cascade of two distillation columns and a membrane unit for the selective separation of H_2O after the first column, as shown in Fig. 3. The main product stream containing

OME_{3-5} exits the subprocess and the streams containing $OME_{<3}$ and $OME_{>5}$ are recycled to the synthesis reactor.

Main reaction network:

$$HO(CH_2O)_nCH_3 + CH_3OH \overset{H^+}{\rightleftharpoons} CH_3O(CH_2O)_nCH_3 + H_2O; \quad n \geq 2 \qquad (14)$$

$$CH_2O + CH_3O(CH_2O)_{n-1}CH_3 \overset{H^+}{\rightleftharpoons} CH_3O(CH_2O)_nCH_3; \quad n \geq 2 \qquad (15)$$

Combustion

A combustion subprocess was implemented to use the energy of the purge streams to produce process steam, which was utilized in the subprocesses. For the simulation of the combustion reactions, an adiabatic Gibbs reactor was applied, and excess air was added accordingly to achieve complete combustion and keep the adiabatic temperature rise below 800 °C. The stoichiometric amount of O_2 required for a complete combustion can be estimated using eqn (16).

Main reaction network:

$$C_xH_yO_z + 1/2(2x + 1/2y - z)O_2 \rightarrow xCO_2 + 1/2yH_2O \qquad (16)$$

Total process routes P1–P4

The combinations thereof lead to production routes P1–P4 of OME. In the following section, each of these total processes are briefly explained.

Process route P1 consists of the subprocesses MeOH synthesis from H_2 and CO_2, FA (aqueous) synthesis and the combination of MeOH and aqueous FA to higher OME synthesis and purification.

Process route P2 consists of the subprocesses MeOH synthesis from H_2 and CO_2 and FA (anhydrous) synthesis, in which H_2 is produced as a by-product and separated and recycled to the MeOH subprocess. Downstream MeOH and anhydrous FA are synthesized to higher OMEs and purified. Almost no H_2O enters the OME_{3-5} subprocess, which reduces the formation of side-products and improves the process energy efficiency associated with smaller recycle streams. However, H_2O is still formed as a by-product in the synthesis of longer chain OMEs and needs to be separated from the recycle stream using a membrane unit.

Process route P3 consists of the subprocesses MeOH synthesis from H_2 and CO_2, FA (aqueous) synthesis and the combination of MeOH and aqueous FA for OME_1 synthesis. OME_1 is further introduced with aqueous FA to the higher OME synthesis and purification. The advantage of P3 is the conversion of MeOH towards OME_1 prior to the synthesis of longer chain OMEs, which allows the separation of a large portion of the H_2O formed before the OME_n synthesis subprocess. In addition, fewer side-products are formed during the synthesis of longer chain OMEs, thereby reducing the energy demand during product purification towards OME_{3-5} and consequently enhancing the process energy efficiency.

Process route P4 consists of the subprocesses MeOH synthesis from H_2 and CO_2, FA (anhydrous) synthesis and the combination of MeOH and anhydrous FA for OME_1 synthesis. OME_1 is further introduced with anhydrous FA to the higher OME synthesis and purification. Hence, this affords the synthesis of longer chain OMEs from H_2O free reactants. This prevents the formation of the side-product H_2O, and thus various other side-products are not formed, which is a very important advantage for the purification of the OME_n reaction product. This is very advantageous given that the recycle of the H_2 side-product of the FA (anhydrous) synthesis leads to significant material and process energy efficiency improvements, in addition to the process energy efficiency improvement potential due to the significantly less purification energy demand in the OME_{3-5} subprocess. More details on process routes P1 to P4 are presented in the ESI.†

4. Methodology

This chapter addresses the general assumptions, system boundaries and methodology of process modelling and simulation, followed by process techno-economic and carbon footprint evaluation methodologies. This is then followed by the description of the comparison criteria.

General assumptions and system boundaries

The system boundaries were set for the evaluation on the simulation level from the feedstock H_2 and CO_2, followed by the synthesis of intermediates up to the desired product OME_{3-5}. It is assumed that the production plant is integrated in a chemical park where the necessary infrastructure for the provision of utilities such as steam and cooling water is available at market prices. CO_2 and H_2 are purchased as waste products or raw materials from renewable non-fossil sources. The waste streams of the processes are wastewater and exhaust gases. The wastewater is treated at market prices, while the exhaust gases are assumed to be released without further treatment. The production of OME_{3-5} consists of several subprocesses, which are altogether material and heat integrated. The obtained distribution of OME chain lengths in the final product OME_{3-5} differs slightly between the investigated process routes. Nevertheless, it is assumed that in all cases, the specification range is fulfilled without further processing and that the heating value

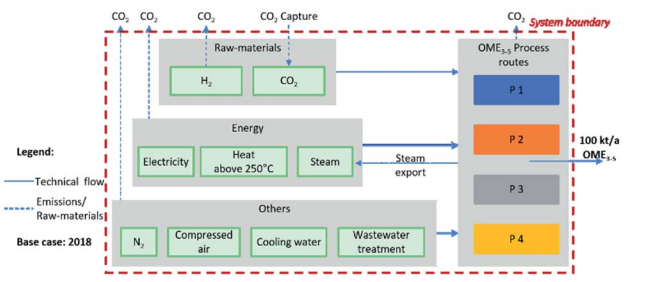

Fig. 4 System boundaries set on the simulation level of the process routes P1–P4.

from Held *et al.*[43] represents the actual heating value as a good approximation. The system boundaries are shown in Fig. 4, and further details on the assumptions are given in the ESI.†

Process modelling and simulation

Steady-state simulations for P1 to P4 were implemented using Aspen Plus® software V11 from Aspen Technology Inc. Aspen Energy Analyzer V11 and Aspen Process Economic Analyzer V11 were used for heat integration and unit operation dimensioning.

The components considered in the simulations were H_2, CO_2, CO, N_2, O_2, FA, MeOH, H_2O, OME_{1-10}, HF_{1-10} and MG_{1-10}. Most of these components such as the acetals, glycols and OME are not included in the standard Aspen database, and thus new components were added in the property analysis environment. An overview of the pure component thermodynamic and thermophysical properties used in the simulations can be found in the ESI.†

To simulate purification processes, in particular thermal separations, interaction parameters are required, which describe the real behaviour of the gas and the liquid phases. For mixtures that contain FA, a UNIFAC-based model was introduced by Maurer *et al.*[54] This model was extended in the following decades by adding new components and by adapting the interaction parameters to new experimental data. Schmitz *et al.*[47] published a new version of the model considering OME_n which was adapted and implemented. An overview of the model and its validation is presented in the ESI.† Adequate model parameter and implementation of the thermodynamic model is crucial for a realistic simulation of this special reactive mixture. A variety of reaction models describing the MeOH, FA (aqueous), FA (anhydrous), OME_1 and OME_n syntheses were used to assess the product compositions exiting the reactors. The models implemented in the simulation environment can be found in the process description of the subprocesses. The synthesis of FA was described based on the conversion and yields from literature values, while the other syntheses were described according to published kinetic models. An overview of the employed reaction models is presented in the ESI.†

Initially, the subprocesses were implemented separately in the simulation platform. Afterwards, the material integration interconnecting these subprocesses to describe process routes P1 to P4 was implemented. The production capacity was adjusted to 100 kt OME_{3-5} per year, and the heat integration was conducted to improve the overall process energy efficiency. Consequently, the heat exchanger network was designed. After the network design, heat exchangers were interconnected in the process simulation to transfer heat from hot streams to cold streams and steam utilities were implemented to consider the steam supply by single process unit operations and the steam demand of other process unit operations. Subsequently, the process components were dimensioned. Based on the simulation material and heat balance, the utilities demand and main operational cost parameters were extracted. Since a complete process route is a combination of several subprocesses, more recycle loops that are interconnected should be converged. Standard numerical solvers in Aspen Plus® were used, while the complex loop convergence of the total process routes was achieved stepwise starting with connecting the subprocesses. After the material integrated loop convergence, heat integration of the total process routes was performed stepwise, followed by convergence of the energy integrated loop. The equipment sizing of unit operations followed the convergence and integration steps using Aspen Process Economic Analyzer V11. For the parameters categorized as non-conventional unit operations, namely, the membranes, heat exchangers, reactors, and the column dimensions for the FA (anhydrous) absorption considered as ideal separation units, literature-based sizing methods were adapted. Membrane areas were evaluated according to the methods described by Schmitz *et al.*[47] and Baker,[64] while the column dimensions were estimated by correlation with the absorption column in the aqueous FA subprocess. A detailed description of the procedure for dimensioning the process components and the heat integration procedure applied for the process routes can be found in the ESI.†

Process evaluation and comparison criteria

The implemented processes P1 to P4 were evaluated using various key performance indicators (KPIs). These KPIs were translated into process evaluation criteria used to compare the process routes, given that they provide a concise summary of the different process routes in terms of mass and energy balance. The process route utility demands and process energy efficiencies were evaluated based on the total mass and energy balance from P1 to P4.

In this work, the energy efficiency of the overall process, η_{energy}, is defined in eqn (17).

$$\eta_{energy} = \frac{\dot{m}_{OME_{3-5}} LHV_{OME_{3-5}}}{\sum_k \dot{Q}_k + \sum_l \dot{W}_l + \sum_i \dot{m}_i LHV_i} \quad (17)$$

where $\dot{m}$ denotes the mass flow rate of the reactants i and the OME_{3-5} containing product stream. LHV is the lower heating value at 298 K, while $\dot{Q}_k$ and $\dot{W}_l$ represent the externally supplied heat fluxes and electric power demand, respectively.

In addition to the energy efficiency of the process routes, the material balance was assessed, and the performance was indicated by two parameters. The first parameter, η_C, reflecting the carbon efficiency, *i.e.*, the ratio of carbon atoms, C, in the feedstock and the carbon atoms in the OME_{3-5} product stream, is defined in eqn (18). The second parameter, η_{mass}, considers the mass flow rates, *i.e.*, the ratio of the OME_{3-5} product mass flow rate with respect to the feedstock mass flow rate, as defined in eqn (19).

$$\eta_C = \frac{C_{OME_{3-5}}}{\sum_i C_i} \quad (18)$$

$$\eta_{mass} = \frac{\dot{m}_{OME_{3-5}}}{\sum_i \dot{m}_i} \quad (19)$$

where $\dot{m}$ denotes the mass flow rate of the reactants i.

Table 1 General assumptions for the economic analysis

Description	Value	Reference
Base year	2018	
Annual full load hours	8000 h per annum	
Plant operation time	20 years	
Plant capacity	100 kt per annum	
Place of location	Germany, Chemical Park	
CO_2 cost, base case	309 € per t_{CO_2}	68
CO_2 cost, variation range	65 to 700 € per t_{CO_2}	Lower limit[69] Higher limit[70]
H_2 cost, base case	4241 € per t_{H_2}	68
H_2 cost, variation range	1500 to 6600 € per t_{H2}	71
LHV_{H_2}	33.3 kW h $kg_{OME_{3-5}}^{-1}$	43
$LHV_{OME_{3-5}}$	5.25 kW h $kg_{OME_{3-5}}^{-1}$	43
LHV_{diesel}	11.9 kW h kg_{diesel}^{-1}	72

Economic evaluation

The methodological approach for production cost estimation is a factorial method described by Peters *et al.*[65] based on the equipment data and material and energy streams obtained from the process simulations. The calculations were carried out with the DLR-inhouse software Techno-Economic Process Evaluation Tool (TEPET) in an automated and standardized manner.[66]

The targeted parameters of the economic analysis are the investment and operating costs as well as the net production costs related to a production unit. An overview of the most important assumptions for the economic evaluation is given in Table 1 (detailed list is given in the ESI†).

The net production costs of fuels from renewable H_2 and CO_2 are typically highly sensitive to the raw material price of the educts.[67] Hence, the future price development exhibits high uncertainty. Consequently, a wide range of CO_2 and H_2 costs was examined to evaluate the influence of cost variations.

Capital expenditures (CAPEX)

CAPEX are calculated based on the purchased equipment costs of the main process equipment. The equipment was categorized as conventional and non-conventional and the sizing data was obtained based on the simulation results explained in the previous section and further explained in the ESI.†

For conventional unit operations, packed columns and shell-and-tube heat exchangers are assumed as equipment types for all applied columns and heat exchangers, respectively. For H_2 compression reciprocating compressors were assumed, while all other compressors were taken as centrifugal-rotary ones. Knock-out drums were considered as storage vessels for the cost calculation.[73] The costs of multistage compressor cooling, absorber cooling and column reboilers and condensers were considered by applying shell-and-tube heat exchanger costs. Reflux pumps were considered separately in the column cost calculation, while the costs for column insulation and connections were neglected. Also, 316 stainless steel was assumed as a standard material due to the presence of FA in the process,[74] except for the burner consisting of carbon steel. For non-conventional unit operations, H_2O membrane plate-and-frame modules were assumed, while the membranes for H_2 separation were taken as hollow-fiber modules in accordance to Baker.[64]

The use of one uniform data base is preferable in the selection of the specific cost for the different types of equipment. Hence, cost functions from Peters *et al.*[65] were applied as appropriate. Specific costs from references other than Peters *et al.*[65] were only chosen in the case of multitube reactors, fixed-bed reactors, thin film evaporators and membrane modules due to the inadequate capacity range or lack of data given in Peters *et al.*[65] A detailed explanation of the deviations from the standard reference and the related assumptions is given in the ESI.† When the capacity limit of the chosen cost function was exceeded, the equipment was separated formally into the minimum number of equally sized components to fit the given range.

Lang factors for fluid processing plants are assumed for the calculation of the additional direct and indirect CAPEX from the purchased equipment cost.[65] Reduced Lang factors for main compressors were assumed considering a reduced share of additional CAPEX in the case of compressors larger than 1000 kW of nominal power. An overall cost factor of 2.27 (compared to 5.93 for all other equipment) was applied.[68] Fixed capital investment (FCI) is calculated from the total direct and indirect cost by assuming an additional share of contractor's fee and contingencies.[65] The total capital investment (TCI) includes a working capital of 15% of the TCI.[65] Annual capital cost (ACC) is determined from the TCI by the annuity method[65] assuming an interest rate of 5%. More details of the methodological approach are described by Albrecht *et al.*[66] All the applied Lang factors are given in the ESI.†

Operational expenditures (OPEX)

For the determination of raw material and utility costs ($OPEX_{R\&U}$) all mass and energy input streams and wastewater output streams and surplus steam provided by the simulation results were considered.

H_2 and CO_2 costs in the base case were taken from generic values,[68] which were calculated following the same assumption basis as in this work. The lower limit of the considered CO_2 cost range was taken from Naims.[69] In this reference, the CO_2 costs for carbon capture from various point sources were examined and a value of approx. 65 € per t_{CO_2} was estimated for a large-scale carbon capture and utilization (CCU) scenario. For the upper limit, a value of 720 € per t_{CO_2} was applied according to House *et al.*[70] for direct air capture (DAC). To the best of our knowledge, this represents the highest CO_2 cost from DAC published to date.[75,76] The H_2 cost ranges were taken from the Hydrogen Europe report[71] considering steam methane reforming (SMR) costs as the lower limit, which are assumed to be the target value for green H_2 costs that could possibly be reached using the proposed optimization strategies. The conservative estimations of electrolysis cost from wind power were taken as the upper limit.[71] The assumed H_2 and CO_2 cost ranges are given in Table 1.

The requirement of high temperature heat (>250 °C) was covered by electrical power, assuming a power-to-heat efficiency of 95% for energy conversion.[77] All catalysts were considered as

raw material streams calculated from the catalyst lifetime. The costs were estimated from the trading price in the case of silver and by extrapolation of low quantity prices on bulk prices in the case of all other catalysts. All other specific costs for raw material and utilities as well as the assumed catalyst lifetimes are given in the ESI.†

Employee-hours per year (h_{labor}) were estimated from the characteristic plant capacity and the number of production steps according to the procedure proposed by Peters *et al.*[65] Specific labor costs for Germany were assumed.[78] Additional direct and indirect operational expenditures ($OPEX_{dir/ind}$) were calculated with the factorial method described by Peters *et al.*[65] and Albrecht *et al.*[66] Given that only the manufacturing costs were determined, no costs for distribution and selling as well research and development were considered. All applied cost factors are given in the ESI.†

Net production costs (NPC)

Specific net production costs (NPC) were calculated from ACC, total OPEX and the product output and related to a litre diesel equivalent (l_{DE}) according to:

$$NPC = \frac{ACC + OPEX_{dir} + OPEX_{ind} + OPEX_{R\&U} + h_{labor}c_{labor}}{\dot{m}_{OME_{3-5}}\frac{LHV_{OME_{3-5}}}{LHV_{diesel} \times \rho_{diesel}}}$$

$$= ACC' + OPEX'_{dir} + OPEX'_{ind} + OPEX'_{R\&U} + C'_{labor} \quad (20)$$

with the output OME_{3-5} mass flow $\dot{m}_{OME_{3-5}}$, the lower heating value $LHV_{OME_{3-5}}$ of OME_{3-5},[43] and the lower heating value LHV_{diesel} and density ρ_{diesel} of diesel.[72]

CO_2 footprint evaluation

LCA is a methodology for evaluating the environmental impacts of product systems along the entire life cycle. LCA is standardized in the ISO 14040/14044 standards[79,80] and considers all environmental impacts of the material and energy flows that are exchanged with the environment.

The carbon footprints of the four process routes P1–P4 for OME_{3-5} were compared by applying a well-to-tank approach. The system boundaries of all routes with feedstock and energy supply are described above and shown in Fig. 4. Note that the CO_2 emissions from the use-phase and end-of-life phase of OME_{3-5} were neglected given that both are identical for all four routes, and thus neutralize each other in a comparison. The construction of chemical plants was neglected in this analysis due to the lack of data.

Comparing technologies consistently requires a common basis. In LCA, this common basis is the so-called "functional" unit.[77] For the well-to-tank approach, we choose "the provision of 1 MJ of enthalpy of combustion" as the functional unit and additionally present the results per litre diesel equivalent. For this study, we focused on evaluating the carbon footprint in the life cycle impact assessment (LCIA) of the four alternative process routes. The environmental impacts were assessed in accordance with the LCIA methodology "ReCiPe Midpoint (H) V1.13 no long-term (LT)" following the methodological guidelines for LCA of synthetic fuels of the research center for energy economics (FfE).[81] Although other impact categories are also relevant, they are beyond the scope of this study.

Table 2 General assumptions for the LCA datasets of H_2, CO_2, and electricity supply in the base case year of 2018 in accordance with the guideline of FfE[81]

Description	Value	Reference
H_2 supply	24.93 kg CO_2-eq. per kg H_2	81
CO_2 supply	−0.76 kg CO_2-eq. per kg CO_2	81
Electricity supply	0.50 kg CO_2-eq. per kW h_{el}	81

For the life cycle inventory (LCI), we considered generic process data of the FfE for H_2, CO_2, and electricity supply, as shown in Table 2.[68] For the electricity supply, we considered today's electricity grid mix in Germany given that it is modelled based on the guideline of FfE. For process heat, we assumed that heat below 250 °C is supplied by steam that is produced as an energy carrier in the chemical industry,[82] while for heat above 250 °C, we assumed an electrode boiler with a power-to-heat efficiency of 95%.[77] Note that processes routes P1, P2, and P4 export steam, for which we consider an environmental credit, *i.e.*, avoided burden, for steam production as energy carrier in the chemical industry.[82] For the H_2 supply, we considered the average carbon footprints of alkaline electrolysis (AEL), solid oxide electrolyser cell (SOEC), and polymer electrolyte membrane (PEM) electrolysis. However, it should be noted that conventional SMR would result in a lower carbon footprint of H_2 supply than electrolysis combined with today's electricity grid mix in Germany. Specifically, the carbon footprint of today's German electricity grid mix, as considered in our base case year of 2018, is considerably high with 24.93 kg CO_2-eq. per kg H_2. Thus, due to this reason, we analyzed the influence of electricity supply on the carbon footprint in a sensitivity analysis, as shown in Fig. 13. CO_2 is supplied by the average of DAC and mono-ethanol amine (MEA) scrubbing in the cement industry. The environmental credit, *i.e.*, avoided burden, for CO_2 utilization is credited to the production of OME_{3-5}.

For additional process data for the supply of utilities such as nitrogen, compressed air, cooling water, and wastewater treatment, we considered LCA datasets of the ecoinvent database.[82] The ESI† presents more details on the used LCA datasets.

Technology readiness level (TRL)

The TRL is defined as a criterion for evaluating the development status of new technologies based on a systematic analysis, which indicates on a scale of 1 to 9 how advanced a technology is. The TRL of the five individual subprocesses and the total process routes P1–P4 was assessed based on the published TRL scale in the Energy Research Program of the German Federal Government addressing the innovations for the energy sector.[83] The TRL scale is presented in the ESI.†

For the purpose of assigning the TRL of the total process routes P1–P4, not only the subprocess with the least TRL was considered to determine the TRL of the total process route, rather we also assigned a mean TRL value for the subprocesses.

Thereby, a better comparison of the TRL of the total process routes is possible. Given that all process routes are limited by individual process components such as the FA synthesis reactor in the FA (anhydrous) subprocess and the H_2O separation unit in the OME_{3-5} subprocess, limiting the TRL of the total process routes to the aforementioned process components would reduce the TRL of P1 to P4 to TRL 3–4, while P1 and P3 would benefit from the high TRL of the FA (aqueous) subprocess. Thus, the mean TRL value allows a realistic presentation of the significant research and development work, which is still to be done to realize the process routes to any considerable extent.

5. Results and discussion

Process simulation and evaluation

Energy and mass balance

After implementing the complete processes in the simulation platform and applying the described methodologies, the results were used for evaluation and comparison. Fig. 5 presents a summary of the results of the mass and energy balance of P1–P4 in the form of e-Sankey diagrams. In addition, the input and output streams are listed in Table 3 with respect to the main product stream OME_{3-5}, accounting for the results of the mass balance at a production of 100 kt per annum OME_{3-5}.

The mass balance evaluation of P1–P4 showed that P1 and P3 require more H_2 and less CO_2 feedstock in comparison to P2 and P4 to produce the targeted 100 kt per annum OME_{3-5}. In fact, this is the outcome of the two different process design concepts for the production of FA relying on aqueous or anhydrous FA. Considering the aqueous routes, they are characterized with a higher production of H_2O, which is the by-product of the acetalization reaction and exits the process as wastewater streams in the case of P1 and P3. Moreover, P1 and P3 have smaller exhaust gas flows due to the use of O_2 as oxidizing agent for the FA (aqueous) subprocess. In contrast, in the FA (anhydrous) subprocess considered in P2 and P4, N_2 is used as a carrier for the

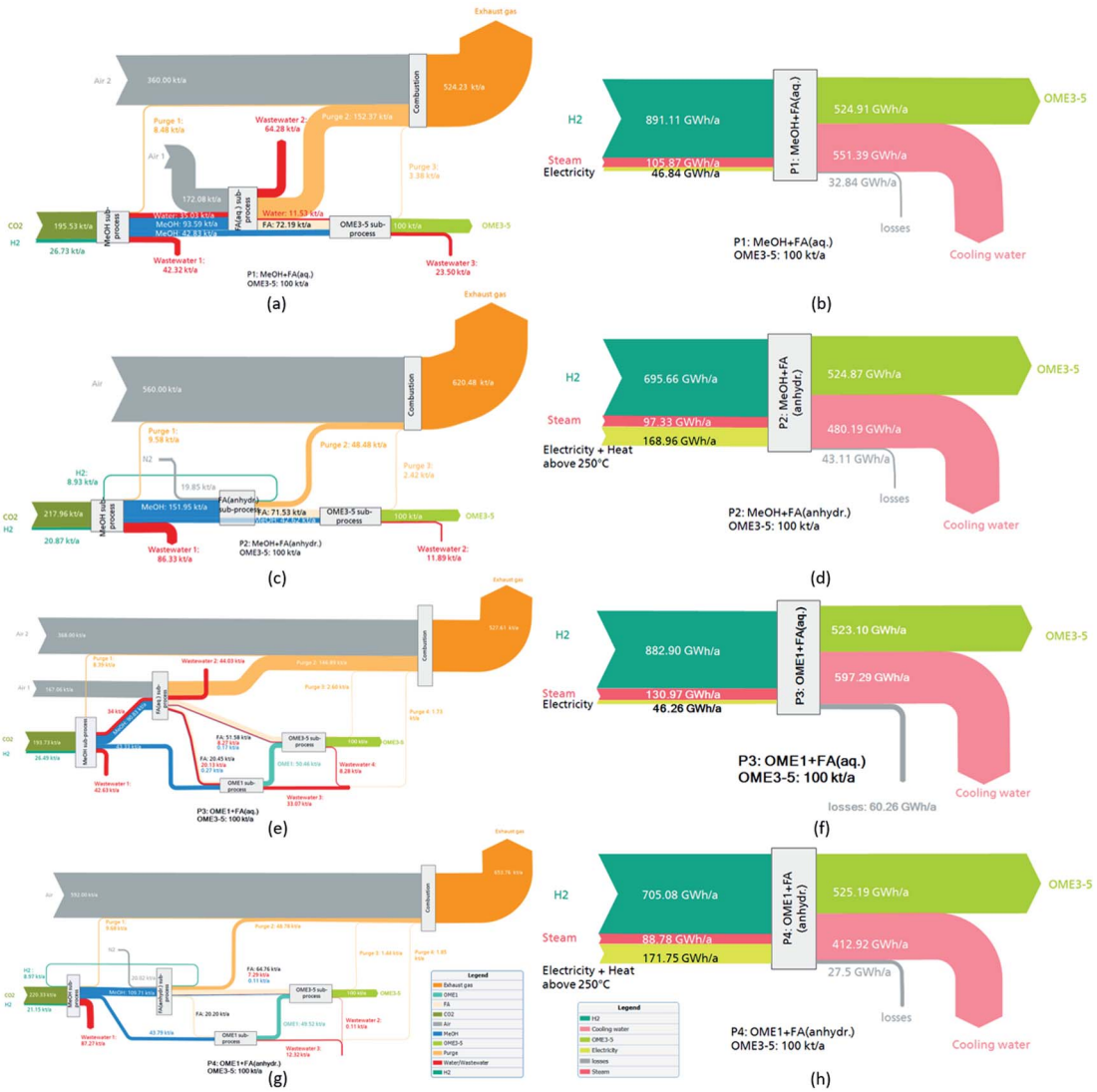

Fig. 5 e-Sankey diagrams for (a) mass balance of P1, (b) energy balance of P1, (c) mass balance of P2, (d) energy balance of P2, (e) mass balance of P3, (f) energy balance of P3, (g) mass balance of P4 and (h) energy balance of P4.

Table 3 Results of the mass balance for P1 to P4 for a production of 100 kt per annum OME_{3-5}

	P1 [kg $kg_{OME_{3-5}}^{-1}$]	P2 [kg $kg_{OME_{3-5}}^{-1}$]	P3 [kg $kg_{OME_{3-5}}^{-1}$]	P4 [kg $kg_{OME_{3-5}}^{-1}$]
Total input	7.54	8.19	7.58	8.53
H_2	0.27	0.21	0.27	0.21
CO_2	1.96	2.18	1.94	2.20
N_2	—	0.20	—	0.20
Air[a]	5.32	5.60	5.37	5.92
Total output	7.54	8.19	7.58	8.53
OME_{3-5}	1.00	1.00	1.00	1.00
OME_3	0.43	0.46	0.44	0.43
OME_4	0.38	0.35	0.36	0.36
OME_5	0.19	0.19	0.18	0.21
Wastewater	1.30	0.98	1.28	1.00
Exhaust gas	5.24	6.21	5.30	6.54

[a] Air used for the FA (aqueous) synthesis and for the combustion of purge streams, while the generated heat was utilized in the processes, as shown in Fig. 3.

Table 4 Results of the energy balance for P1 to P4 for a production of 100 kt per annum OME_{3-5}

	P1 [kW h kW $h_{OME_{3-5},\,LHV}^{-1}$]	P2 [kW h kW $h_{OME_{3-5},\,LHV}^{-1}$]	P3 [kW h kW $h_{OME_{3-5},\,LHV}^{-1}$]	P4 [kW h kW $h_{OME_{3-5},\,LHV}^{-1}$]
Total input				
H_2	1.70	1.33	1.69	1.34
Total output				
OME_{3-5}	1.00	1.00	1.00	1.00
Energy demand				
Electricity	0.09	0.13	0.09	0.14
Steam, 4 bar	−0.10	−0.07	0.09	0.24
Steam, 20 bar	0.30	0.26	0.16	−0.07
Cooling water, 15–20 °C	−0.19	—	−0.19	—
Cooling water, 15–25 °C	−0.86	−0.91	−0.92	−0.79
Heat, T > 250 °C	—	0.19	—	0.19

feedstock MeOH, which should be introduced at certain dilution to the FA reactor. As a result of purging a portion of the carrier gas to prevent the accumulation of the side product CO, the FA (anhydrous) subprocess has a higher exhaust gas flow. In addition, the side product CO of the FA (anhydrous) subprocess leads to a higher demand of CO_2 for P2 and P4. Alternatively, the H_2 side-product of the endothermic MeOH dissociation reaction in the anhydrous FA synthesis – which is recycled to the MeOH synthesis – lowers the demand for the total process H_2 feedstock in comparison to P1 and P3. Consequently, this results in higher input and output mass flows for P2 and P4. In addition, the OME_3, OME_4 and OME_5 compositions reveal small differences between the process routes. However, the study here focused on similar product compositions rather than minimal recycle flows to define the feedstock composition of the OME_{3-5} subprocess. This approach is based on the assumption that product composition is of greater importance to the application than the process energy efficiency of the production process.

Table 4 shows the energy flows of the input and output streams relative to the energy flow of the product stream OME_{3-5} for P1–P4. The energy flow is expressed as the product of LHV and mass flow. In addition, the energy demands in terms of electricity, steam, cooling water and heat utilities above 250 °C are shown relative to the OME_{3-5} product stream.

The energy balance of the considered process routes shows that P2 and P4 require more electricity, which is mainly due to the higher energy demand at the high temperature level > 250 °C for the synthesis of FA (anhydrous). Additionally, the higher dilution rate required for the successful conversion of MeOH to FA and H_2 increases the demand for the compression recycling of the carrier gas stream.

Moreover, P1, P2 and P4 show negative steam demands in the case of 4 or 20 bar, which is mainly due to the fact that the

Table 5 Results of the process efficiencies for P1 to P4 and literature results[40,41,43]

	P1 [%]	P2 [%]	P3 [%]	P4 [%]	Literature
η_{energy}	50.3	54.6	49.3	54.4	31–60
η_C	81.6	73.2	82.1	72.5	
η_{mass}	38.1	41.9	38.5	41.4	

steam generated in the MeOH synthesis reactor is used to supply the heat to the reboilers in the OME_{3-5} subprocess. This effect was also elaborated by Schemme *et al.*[40] In addition, different feedstocks for the OME_{3-5} subprocess result in different mass flows being fractionated in the distillation columns due to the formation of side-products, which in turn leads to different reboiler and condenser duties. The absorber of the FA (aqueous) subprocess requires cooling water with maximum temperature rise of up to 20 °C. Overall, P1 and P3 show a lower electricity demand and higher steam and cooling water demand but no demand for heat above 250 °C.

Process efficiencies

Based on the methodology discussed in Section 3, different process energy and material efficiencies were evaluated and the results are listed in Table 5 and presented in Fig. 6.

Process routes P2 and P4 comprising the anhydrous FA synthesis subprocess exhibit the highest energetic efficiencies due to the recycling of the valuable side product H_2 as a feedstock. In contrast, P2 and P4 exhibit lower carbon efficiencies principally due to the side reaction in the synthesis of FA (anhydrous) to CO. Evidently, as shown in Table 4, the lower energetic efficiencies of P1 and P3 arise principally from the higher H_2 demand, which is not fully compensated for by the heat required at above 250 °C in P2 and P4. The lower overall material efficiency, η_{mass}, of the feedstock being converted to OME_{3-5} for P1 and P3 is a result of the production of large amounts of the side product H_2O in the synthesis of FA (aqueous) due to the MeOH partial oxidation reaction. This generated H_2O is separated with large effort downstream to the FA (aqueous) subprocess and leaves the process in the form of wastewater.

Held *et al.*[43] investigated different scenarios to produce OME_{3-5} based on stoichiometric material balances together with different heat integration strategies within the subprocesses and carbon capture scenarios for the feedstock CO_2. Particularly, one scenario allows for heat integration between all subprocesses in combination with CO_2 from point sources (CPS) assuming CO_2 is available for zero incremental energy costs. This scenario is consistent with our CO_2 feedstock assumptions, which consider purchasing already prepared CO_2 without extending the system boundaries to include the separation and preparation of CO_2. Under this scenario, a process energy efficiency of 59–60% was estimated, which is slightly higher than the process energy efficiency estimated in this work. The difference is particularly a result of the different level of detail considered for the process simulation in both studies. Schemme *et al.*[40] and Burre *et al.*[41] also investigated different routes to produce OME_{3-5} based on H_2 feedstock. However, in these studies, a process energy efficiency of 31–40% was estimated, which is significantly lower than that estimated in this work, being closer to the results from the scenario reported Held *et al.*,[43] in which heat integration is only considered within the subprocesses themselves rather than within the entire process chain. Hence, this highlights the impact and importance of heat integration on process energy efficiency with respect to the entire process route. Specifically, the effect of using the surplus heat from the MeOH subprocess throughout the entire process heat integration has a positive impact on the process energy efficiency.

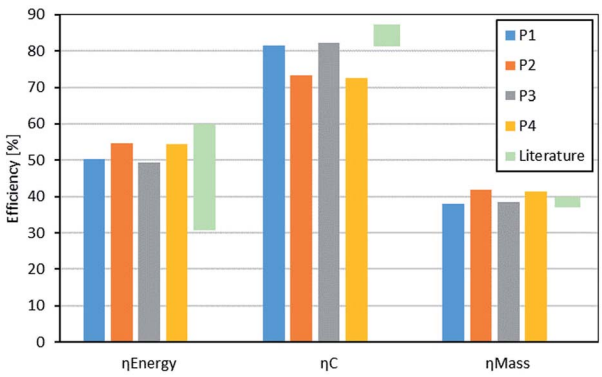

Fig. 6 Results of the process efficiencies for the process routes P1 to P4.

Economic evaluation

CAPEX base case

An overview of the calculated CAPEX is given in Table 6. The obtained purchased equipment cost (EC) differs significantly, ranging from 28 Mio€ in the case of P3 up to 49 Mio€ in the case of P2.

Table 6 Calculated CAPEX for process routes P1–P4

	P1	P2	P3	P4
EC [Mio€$_{2018}$]	29	49	28	40
FCI [Mio€$_{2018}$]	128	215	126	182
ACC [Mio€$_{2018}$ per annum]	11	19	11	16

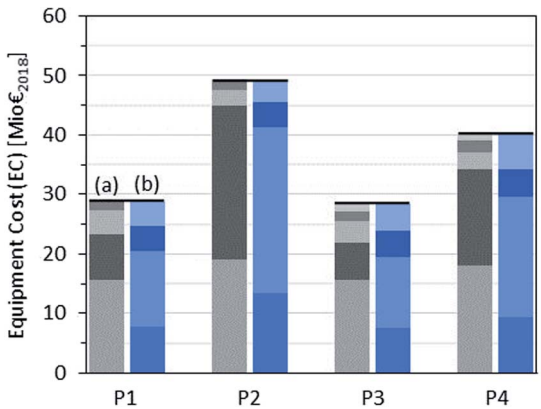

Fig. 7 Breakdown of the equipment costs of routes P1–P4 (a) by synthesis steps, left grey column from bottom to top: MeOH, FA (aqueous or anhydrous), OME_{3-5}, heat recovery, and OME_1 (only P3 and P4) and (b) by equipment type, right blue column from bottom to top: compressors, heat exchangers, reactors, and separators. The marginal contribution of pump costs is not visible in this diagram.

Table 7 Calculated OPEX for routes P1–P4

	P1 [Mio€$_{2018}$ per annum]	P2 [Mio€$_{2018}$ per annum]	P3 [Mio€$_{2018}$ per annum]	P4 [Mio€$_{2018}$ per annum]
$OPEX_{R\&U}$	194	177	193	179
Labor costs	4.2	4.2	5.4	5.9
$OPEX_{dir}$	4.4	6.4	4.8	6.2
$OPEX_{ind}$	6.4	8.7	7.2	9.0
$OPEX_{tot}$	209	196	210	197

The contribution of the different process steps and the different types of equipment to the overall equipment cost is shown in Fig. 7. The main contributors are the MeOH and FA (aqueous/anhydrous) subprocesses in all routes. With respect to the equipment type, compressors and heat exchangers exhibit generally the highest share of equipment costs. The marginal contribution of the pump costs amounts to less than 1% for all routes.

The elevated EC of routes P2 and P4 result mainly from the FA (anhydrous) subprocess, while the EC of all the other process steps only differs slightly between the different routes. Remarkably, the additional OME_1 subprocess of routes P3 and P4 does not lead to a significant increase in EC compared to routes P1 and P2 without an OME_1 step. The high EC of the FA (anhydrous) subprocess can be explained by the elevated reaction temperature (900 °C) compared to the FA (aqueous) subprocess (650 °C) and the additional separation and recycle of H_2 to the MeOH subprocess involving compression from 2 to 29 bar. This leads to larger heat exchanger areas and a higher demand of compression work in comparison to the FA (aqueous) subprocess, and therefore higher costs for heat exchangers and compressors. A detailed breakdown of the calculated EC is given in the ESI.†

In total, the calculated FCI ranges from around 130 Mio€ in the case of P1 and P3 to 215 Mio€ for P2, resulting in an ACC between 11 Mio€ per annum and 19 Mio€ per annum.

OPEX base case

Table 7 gives an overview of the calculated OPEX. The main contributors to the overall operational costs are $OPEX_{R\&U}$, while labor costs and other direct and indirect OPEX only contribute to around 10% in total.

A breakdown of $OPEX_{R\&U}$ is shown in Fig. 8. As expected, the CO_2 and H_2 costs have the greatest impact on $OPEX_{R\&U}$, which range from 60 Mio€ per annum (P1/P3) to 68 Mio€ per annum (P4) for CO_2 and 89 Mio€ per annum (P2) to 113 Mio€ per annum (P1) for H_2 in the base case. The lower H_2 costs in P2 and P4 compared to P1 and P3 result from the FA (anhydrous) subprocess, which allows a higher H_2 efficiency given that less or no H_2O is generated as a side product. However, the savings are diminished by the somewhat higher CO_2 demand in P2 and P4 due to the considerable amount of CO formed as by-product, which leads to higher purge rates in the synthesis of FA (anhydrous).

The residual $OPEX_{R\&U}$ amounts to around 15 Mio€ per annum for all the routes. The main contributors are steam, compressed air, and electricity, as well as the silver catalyst in the case of P1 and P3. It should be noted that silver catalysts can be regenerated electrolytically with negligible material and activity loss.[60,84] This may lead to a reduction in the silver catalyst costs. However, due to its low overall impact, the consideration of silver regeneration was beyond the scope of the present work. Selling of excess heat in P1, P2 and P4, which cannot be integrated into the processes, only leads to minor revenue compared to the overall utility cost. A detailed breakdown of the calculated $OPEX_{R\&U}$ is given in the ESI.†

NPC base case

A breakdown of the NPC is shown in Fig. 9. The lower CAPEX of P1 and P3 is compensated by the somewhat higher raw material cost. In general, raw material costs have a much higher impact on the NPC than CAPEX.

The calculated NPC amounts to 4.14 €$_{2018}$ per l_{DE} for P1, 4.05 €$_{2018}$ per l_{DE} for P2, 4.18 €$_{2018}$ per l_{DE} for P3 and

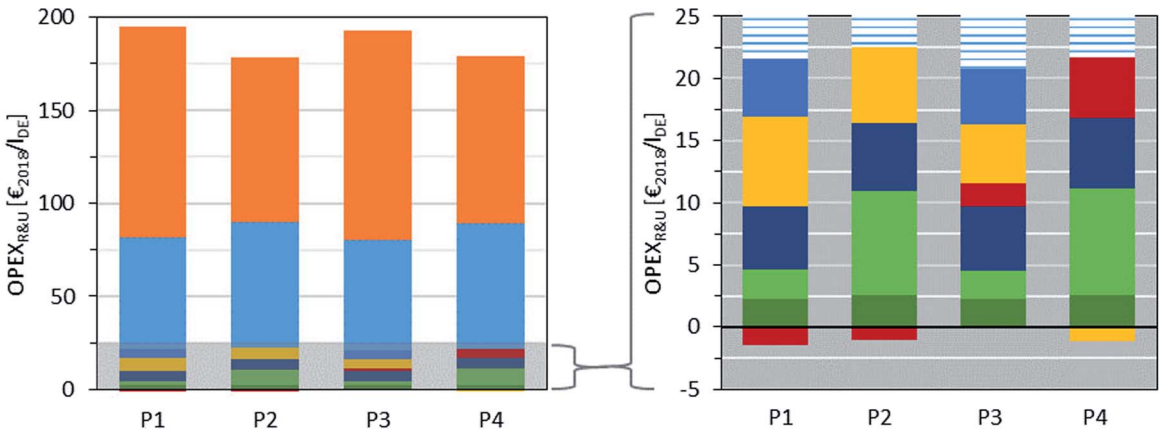

Fig. 8 Breakdown of raw material and utility R&U costs of routes P1–P4: ■ H_2, ■ CO_2, ■ silver (FA, aqueous), ■ 20 bar steam, ■ 4 bar steam, ■ compressed air, ■ electricity, and ■ remaining costs.

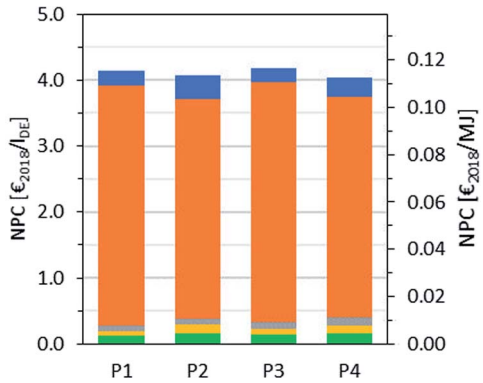

Fig. 9 Breakdown of net production costs (NPC) of routes P1–P4: ACC′, $OPEX'_{R\&U}$, C'_{labor}, $OPEX'_{dir}$, and $OPEX'_{ind}$.

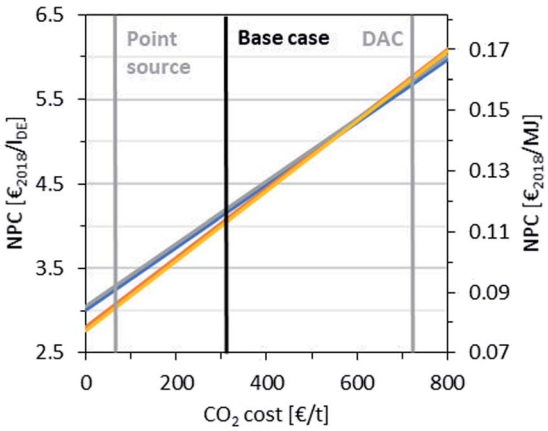

Fig. 10 Dependence of NPC on the CO_2 cost: P1, P2, P3 and P4. Point source cost from ref. 69 and DAC cost from ref. 70. All other raw material costs are fixed as in the base case.

4.05 €$_{2018}$ per l_{DE} for P4. However, it should be note that the deviations are small considering the uncertainty of the net production cost estimation.[66]

Variation of CO_2 and H_2 price

The NPC was calculated for a wide range of CO_2 and H_2 costs to examine the influence of the variability of future price developments. The results are shown in Fig. 10 and 11 for a variation in the CO_2 and H_2 cost, respectively, fixing the other raw material costs as in the base case. This is extended in Fig. 11 (right), where the H_2 cost is varied against different CO_2 cost scenarios, covering a wide range of production locations worldwide and business cases. The high dependency of the NPC on the CO_2 and H_2 price is illustrated. In the case of a CO_2 cost variation, an NPC of between 3.0 € per l_{DE} and 5.8 € per l_{DE} is obtained, while a variation in the H_2 price leads to an NPC of 2.8 to 5.4 € per l_{DE}.

The maximum discrepancy between the different routes is observed at the lower limit of the CO_2 cost range between P3 (3.3 € per l_{DE}) and P4 (3.0 € per l_{DE}) and at the higher limit of the H_2 cost range between P2/P4 (5.0 € per l_{DE}) and P3 (5.4 € per l_{DE}). However, these discrepancies with a maximum of 10% are still small considering the uncertainties and the rational assumptions made. Additionally, Fig. 11 (right) represents P4 for the variation in the CO_2 cost with the variable H_2 cost. Hence, the NPC ranges from 1.7 € per l_{DE} and 6.7 € per l_{DE}. In contrast, the dashed green line represents the highest NPC of P4 with variable H_2 cost and a DAC price of 720 € per t_{CO_2},[70] where the price range for carbon capture with DAC technology is currently subject to great uncertainties, ranging from 100 to 800 € per t_{CO_2}.[85]

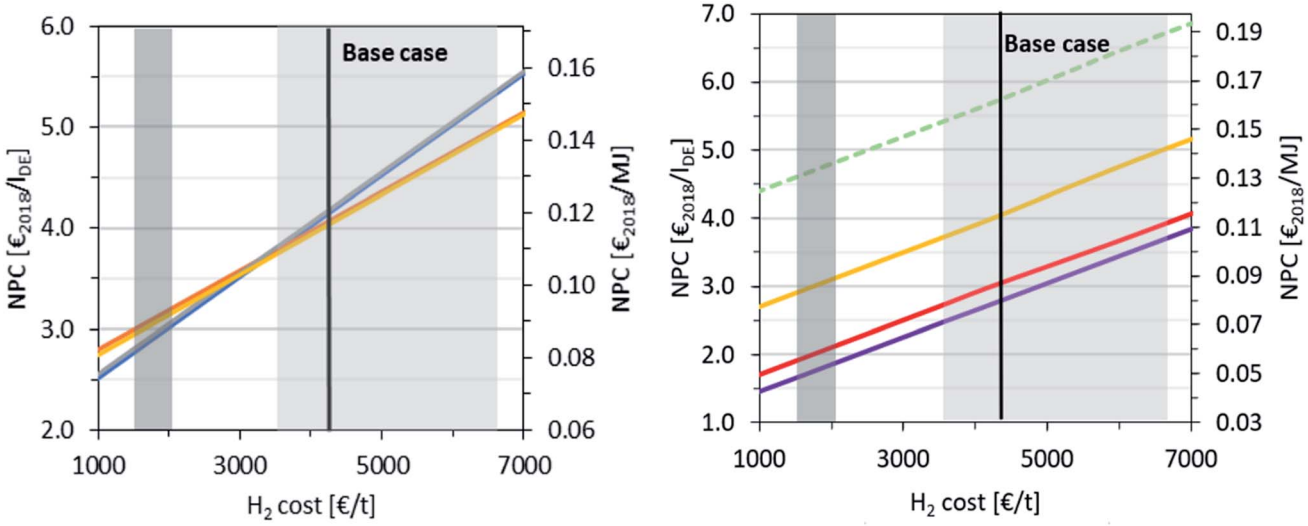

Fig. 11 (Left) Dependence of NPC on the H_2 cost: P1, P2, P3, P4 dark grey shaded area: SMR cost range representing a prospective lower limit of green H_2 cost according to ref. 71 and light-grey shaded area: wind power-based electrolysis cost range from ref. 71. All other raw material costs are fixed on the base case. (Right) Dependence of NPC on the H_2 and CO_2 cost: P4 at 0 € per t_{CO_2} (available CO_2 in-site), P4 at 62 € per t_{CO_2} (MEA_{2018} cost from ref. 68), P4 base case, P4 at 720 € per t_{CO_2} (DAC_{2018} cost from ref. 70); dark grey shaded area: SMR cost range representing a prospective lower limit of green H_2 cost according to ref. 71, light-grey shaded area: wind power-based electrolysis cost range from ref. 71.

Discussion of economic results

CAPEX, OPEX and NPC were calculated for the different production routes presented in this work. The main differences in the cost structure were observed for the different approaches for the synthesis of FA (aqueous/anhydrous). Firstly, the higher investment cost for heat exchangers in the FA (anhydrous) subprocess results from its high reaction temperatures. This cost could be diminished by milder process conditions which is a matter of further R&D efforts. Secondly, differences arise from the fact that in the FA (anhydrous) subprocess, H_2 is formed and recycled back to the MeOH subprocess. The recycling leads to somewhat higher investment costs for compressors, but higher H-efficiency, and consequently lower H_2 costs. These savings in OPEX, which have a much higher impact on the NPC, exceed the additional CAPEX significantly. Nevertheless, no significant differences in the overall NPC of the different routes were obtained over the whole considered parameter ranges. Consequently, no route is clearly preferable from an economic point of view. A preference can be obtained from weighing the different relations of CAPEX and OPEX resulting from the different FA subprocesses.

To the best of our knowledge, there is one peer-reviewed study in the literature that conducted a techno-economic assessment of OME_{3-5} production from H_2 and CO_2 as feedstock.[40] Other publications deal with OME production from biomass[86,87] or MeOH[88,89] as feedstock, and thus are not directly comparable to this work.

In the study by Schemme *et al.*,[40] the production routes of different oxygenated alternative fuels were studied analyzing the process efficiencies and production cost. The methodology for the economic evaluation and system boundaries are similar to the approach applied in this work, however the rigorosity and level of detail of the process simulation is extended in this work. Hence, a comparison between the economic results from Schemme *et al.*[40] and this work was carried out. To achieve a comparable data basis, the framework assumptions from Schemme *et al.*[40] were applied as much as possible to the model in this work. This was mainly the case for the base year, interest rate and $LHV_{OME_{3-5}}$ as well as the CO_2, H_2, steam and electricity costs.

Primarily, no adaptions could be made for the plant capacity, CO_2 feed conditions, cooling water and steam conditions, compressor and pump efficiencies and pressure losses. A detailed comparison of the assumptions of Schemme *et al.*[40] and this work and the results of the comparative calculations are given in the ESI.† Applying the assumptions made by Schemme *et al.*[40] to the model from this work results in an NPC of 3.67 € per l_{DE} for route P1 compared to 3.46 € per l_{DE} obtained by Schemme *et al.*[40] ("Route A" in ref. 40), which corresponds to a deviation of 6%. Hence, an agreement of the NPC of route P1 can be stated in the error range of the calculations. Moreover, it can be concluded that the novel OME production routes P2 to P4 studied in this work are competitive to the TRI routes ("Route B" and "Route C") considered by Schemme *et al.*[40]

Carbon footprint evaluation

Contribution analysis base case

In the base case year of 2018, the carbon footprints of process routes P1 and P3 are around 0.35 kg CO_2-eq. per MJ, and thus significantly higher than the carbon footprints of P2 and P4 with about 0.30 kg CO_2-eq. per MJ (Fig. 12 and the ESI†). Therefore, we compared the hotspots in the OME_{3-5} supply chain using P3 and P4 (Fig. 12) as examples in the proceeding contribution analysis.

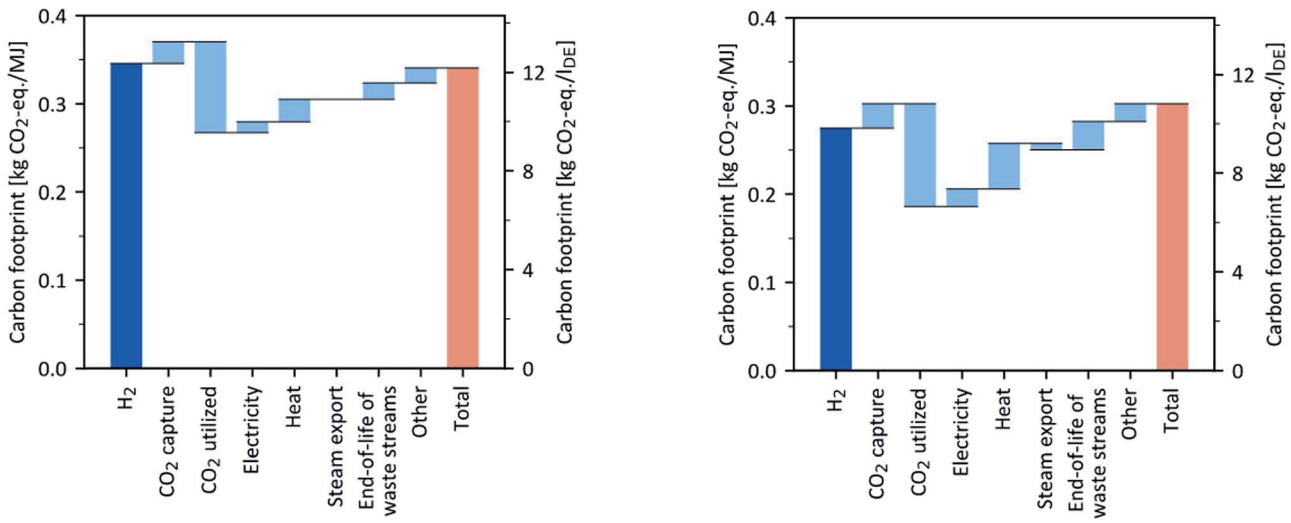

Fig. 12 Contribution analysis of the carbon footprint of the OME_{3-5} routes P3 (left) and P4 (right) for year 2018. The left *y*-axis shows the carbon footprint in kg CO_2-eq. per MJ, while the right *y*-axis additionally indicates results in kg CO_2-eq. per l_{DE}. The end-of-life of waste streams considers CO_2 in the exhaust gas and carbon carriers in the wastewater. Minor emissions due to wastewater treatment and the supply of cooling water, nitrogen, and compressed air are summarized as "other".

The carbon footprints of OME_{3-5} production are mostly driven by H_2 and CO_2 supply for both routes P3 and P4, as shown in Fig. 12. Most emissions arise from H_2 supply, which is produced by electrolysis *via* today's electricity mix in the base case. Note that in P4, the H_2 supply contributes less to the carbon footprint than in P3 (Fig. 12) given that P4 requires 20% less H_2 per kg OME_{3-5} than P3. The environmental credit, *i.e.*, avoided burden, for utilized CO_2 strongly reduces the carbon footprint of both P3 and P4. However, in P4, the environmental credit for CO_2 utilization is higher than that of P3, given that P4 requires 13% more CO_2 per kg of produced OME_{3-5} due to its lower carbon selectivity towards OME_{3-5} in comparison to P3. Thus, the higher amount of utilized CO_2 in P4 is converted into more carbon carriers in waste streams, *i.e.*, wastewater and exhaust gas (Fig. 12).

Although P4 is credited for its steam export, the heat supply in P4 contributes roughly twice as much to the carbon footprint as in P3 (Fig. 12). In contrast to P3, P4 additionally requires high-temperature heat above 250 °C, which is supplied electricity-based *via* an electrode boiler.

Overall, the carbon footprint depends strongly on the carbon footprint of electricity supply if electricity-based H_2 and high-temperature heat are used. Therefore, we also investigated the influence of the carbon footprint of electricity supply on the carbon footprint of the OME_{3-5} product for all four process routes in a sensitivity analysis.

Sensitivity analysis for carbon footprint of electricity supply

In this sensitivity analysis, the carbon footprint of OME_{3-5} is minimized in a supply chain optimization as a function of the carbon footprint of electricity supply, as shown in Fig. 13. For the supply chain optimization, conventional, fossil-based H_2 and high-temperature heat supply *via* steam methane reforming[90] and a natural gas boiler,[82] respectively, are included as alternatives to the PtX technology electrolysis and electrode boiler of the base case. The tipping point between a fossil-based and PtX supply chain is reached at a carbon footprint of electricity supply of 220 g CO_2-eq. per kW h_{el}. Above 220 g CO_2-eq. per kW h_{el}, the supply chain optimization results in fossil-based H_2 and high-temperature heat supply given that a PtX supply chain would result in a much larger carbon footprint (Fig. 13, grey dotted lines).

In contrast, H_2 and high-temperature heat are supplied by PtX technologies below 220 g CO_2-eq. per kW h_{el}. With an electricity carbon footprint below 56 to 68 g CO_2-eq. per kW h_{el}, the production of OME_{3-5} is carbon negative. Please note that this negative carbon footprint only considers the system boundaries of OME_{3-5} production, where the combustion of OME_{3-5} releases CO_2, making the entire life cycle of OME_{3-5} carbon neutral in a complete WtW (cradle-to-grave) scope. When wind power is used for electricity supply, the carbon footprints of the OME_{3-5} production are about −36 g CO_2-eq. per MJ, which is in good agreement with the results of Hank *et al.*[10] for low-carbon electricity supply. Thus, with today's power grid mix, a fossil-based OME_{3-5} supply chain would be more environmentally friendly in terms of the carbon footprint. Overall, the OME_{3-5} routes P2 and P4 have the lowest carbon footprint independent of the carbon footprint of electricity supply.

Sensitivity analysis for carbon footprint of CO_2 and H_2 supply

The sensitivity of the OME_{3-5} carbon footprint towards the supply of both raw materials CO_2 and H_2 was also investigated. In the case of the sensitivity analysis for CO_2 supply (Fig. 14), DAC (light grey) and MEA cement (dark grey) were analysed for the years 2018 and 2050, in accordance with the generic process data of the FfE.[81] Processes P2 and P4 yield lower carbon footprints than P1 and P3, irrespective of the CO_2 supply.

In case of the sensitivity analysis for H_2 supply (Fig. 15), generic process data for H_2 supply *via* electrolysis of the FfE is

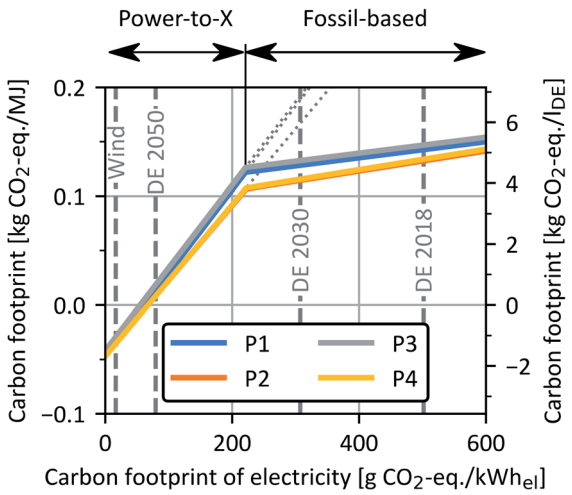

Fig. 13 Carbon footprint of all four OME_{3-5} process routes as a function of the carbon footprint of electricity supply for the base case. The left *y*-axis shows the carbon footprint in kg CO_2-eq. per MJ, while the right *y*-axis additionally indicates results in kg CO_2-eq. per l_{DE}. Wind: wind power, DE 2018/2030/2050: German power grid mix 2018/2030/2050.[68]

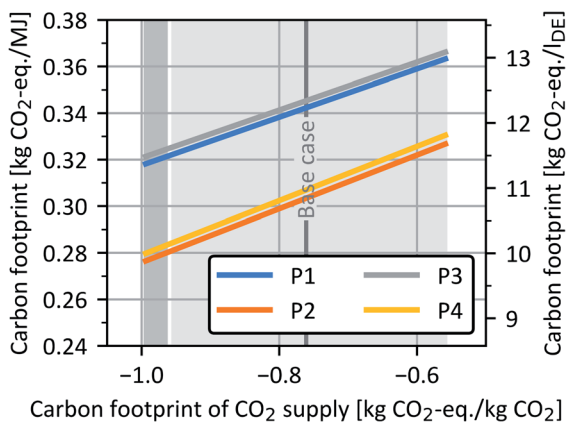

Fig. 14 Carbon footprint of all four OME_{3-5} process routes as a function of the carbon footprint of CO_2 supply. The left *y*-axis shows the carbon footprint in kg CO_2-eq. per MJ, while the right *y*-axis additionally indicates results in kg CO_2-eq. per l_{DE}. The shaded areas indicate the carbon footprint ranges of CO_2 supply from DAC (light grey) and MEA cement (dark grey) for the years 2018 and 2050.[68]

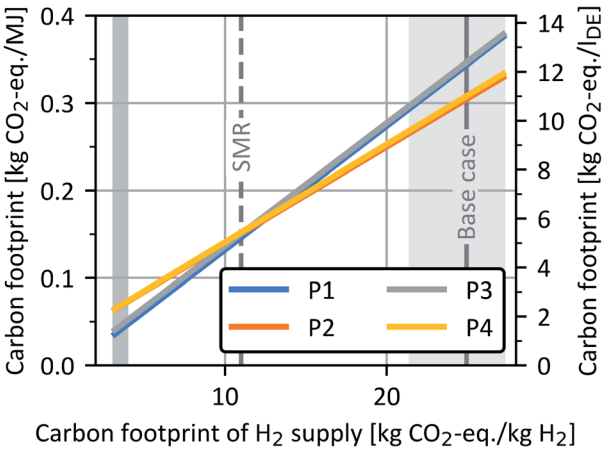

Fig. 15 Carbon footprint of all four OME_{3-5} process routes as a function of the carbon footprint of H_2 supply. The left *y*-axis shows the carbon footprint in kg CO_2-eq. per MJ, while the right *y*-axis additionally indicates the results in kg CO_2-eq. per l_{DE}. The shaded areas indicate the carbon footprint ranges of H_2 supply for the years 2018 (light grey) and 2050 (dark grey).[68] SMR: steam methane reforming.

considered for the years 2018 (light grey) and 2050 (dark grey). With the generic process data for 2018 (light grey), processes P2 and P4 yield the lowest carbon footprints. In contrast, when the generic process data for 2050 (dark grey) or SMR is considered, processes P1 and P3 have lower carbon footprints than P2 and P4. With this clean H_2 supply in 2050, the higher heat consumption of P2 and P4 becomes more decisive and leads to higher carbon footprints in both processes in this case.

In the ESI,† we additionally present the sensitivity analyses for the carbon footprint of high-temperature heat supply as well as the environmental credit, *i.e.*, avoided burden, for steam exports. The additional sensitivity analyses show that process routes P2 and P4 yield lower carbon footprints compared to process routes P1 and P3 irrespective of the considered ranges of high-temperature heat supply and the environmental credit for steam exports.

Technology readiness level (TRL)

The TRLs assigned to the five individual subprocesses and the entire process routes P1 to P4 are shown in Table 8.

Table 8 TRL results of the subprocesses and P1 to P4

Subprocess	TRL
MeOH	9
FA (aqueous)	9
FA (anhydrous)	3–4
OME_1	9
OME_{3-5}	3–4
Total process	
P1	3–7
P2	3–5
P3	3–8
P4	3–6

The MeOH subprocess based on H_2 and CO_2 feedstocks exists on a large scale.[91] Hence, it has a TRL of 9. Identical assumptions were made by Schemme *et al.*,[40] and Bardow *et al.*[92] also cites a high TRL for this technology.

On the one hand, the FA (aqueous) subprocess also exists on a large scale.[60] Hence, it has a TRL of 9. On the other hand, the FA (anhydrous) subprocess requires more research and demonstration steps to achieve the same TRL. In fact, the proof of concept was validated in several laboratory experiments.[42,62,93] However, besides these studies, to the best of our knowledge, long-term experiments and scale-up plants have not been implemented to date. Hence, a TRL of 3–4 was assigned to this subprocess.

The OME_1 subprocess was investigated by Drunsel *et al.*, working on a laboratory-scale distillation column.[63,94] In addition, a plant that produces OME_1 on a large scale was commissioned following the process concept of Drunsel *et al.* Hence, it has a TRL of 9.[95,96] Schemme *et al.*[40] also investigated the subprocess assuming a TRL of at least 5.

Different feedstocks are used for the OME_{3-5} subprocess, resulting in the need for adjustments, particularly for the reactor, distillation columns and the H_2O separating process unit. However, previous studies have been conducted with regard to the reaction, distillation and H_2O separation for specific mixtures, some of which are very similar to the mixtures assessed in this work, and a demonstration plant[97] was built and commissioned in the scope of the NAMOSYN project. Therefore, the TRL was assumed to be 3–4. If the demonstration plan shows promising results during long-term test runs regarding the performance of the critical process components, the TRL can be assigned higher values.

The TRL for P1–P4 is presented in two ways. The first number indicates the lowest TRL of the considered subprocesses, and therefore is equal to 3 for all four process routes. Given that this only shows the main hurdle of the entire process chain, but does not show the advantages of the individual subprocesses, the second number presents the mean TRL of the subprocesses. This is much higher for all four process routes, where a difference between P1 and P3 with a TRL 7 and 8 is observed in comparison to P2 and P4 with a TRL 5 and 6. This is a result of the low TRL of the FA (anhydrous) subprocess in comparison to the FA (aqueous) subprocess. Due to the beneficial results of P2 and P4 regarding process efficiency and carbon footprint, further investigations to improve the TRL of FA (anhydrous) should be carried out.

An overview of the process evaluation criteria for the considered processes in web diagrams for the years 2018, 2030 and 2050 is available in ESI Fig. S12–S14.†

6. Conclusions

Based on a standardized and validated modelling and simulation methodology implemented in Aspen Plus®, four different process routes for the production of OME_{3-5} were evaluated considering techno-economic assessment and carbon footprint. The evaluated processes are based on scalable technologies, which have the potential to achieve a feasible large-scale OME

production. The feedstock for all four routes P1–P4 are CO_2 and H_2 to enable the sustainable production of the first intermediate product MeOH. Different subprocesses follow to prepare the intermediates for the synthesis of OME_n, *i.e.* FA (aqueous) with MeOH for P1, FA (anhydrous) with MeOH for P2, FA (aqueous) with OME_1 for P3 and FA (anhydrous) with OME_1 for P4. Subsequently, OME_{3-5} are synthesized and purified on the scale of 100 kt OME_{3-5} per year. The base case was considered under the German boundary conditions for the year 2018. All processes were energy integrated along the process chain starting from H_2 and CO_2 with the target of maximizing the energy recovery. Based on the material and heat balance results, the overall energy efficiency evaluated for the different processes varied between *ca.* 50–55%. Processes based on anhydrous FA (P2 and P4) showed a trend of higher energy efficiency due to the reutilization of the H_2 by-product from the MeOH endothermic dissociation reaction in the MeOH synthesis loop. From an economic point of view, the calculated NPC under the base case conditions (cost of H_2 of 4241 € per t_{H_2} and cost of CO_2 of 309 € per t_{CO_2}) amounts to 4.14 $€_{2018}$ per l_{DE} for P1, 4.05 $€_{2018}$ per l_{DE} for P2, 4.18 $€_{2018}$ per l_{DE} for P3 and 4.05 $€_{2018}$ per l_{DE} for P4. No significant differences in the overall NPC of the different routes were obtained over the whole considered parameter ranges. This is due to the trade-off between the CAPEX and OPEX, which occurred due to the lower cost of the feedstock for the anhydrous FA-based processes P2 and P4, while having a higher CAPEX mainly due to the high temperature endothermic methanol dissociation reaction at low MeOH concentrations. The high dependency of the NPC on the CO_2 and H_2 costs was illustrated using a sensitivity analysis. In the case of CO_2 cost variation (at H_2 base case cost), the NPC of OME between 3.0 € per l_{DE} and 5.8 € per l_{DE} was obtained, while a variation in the H_2 price (at CO_2 base case cost) led to an NPC 2.8 to 5.4 € per l_{DE}. The combination of OME production based on the CO_2 point source feedstock cost and H_2 cost provisioned future production using cheap renewable electricity (at H_2 price of ≤2438 € per t from AEL in 2050 and CO_2 price of ≤62 € per t from MEA, cement) can significantly reduce the costs for sustainable OME production at ≤2.33 € per l_{DE}. In the case of CO_2 feedstock available onsite at no price, the OME production cost under 2 € per l_{DE} can be achieved with green H_2 produced under favored conditions at ≤2000 € per t_{H_2}.

The carbon footprints of OME_{3-5} production are mostly driven by H_2 and CO_2 supply for both anhydrous (P4)- and aqueous FA (P3)-based routes. In the base case in the year 2018, the carbon footprint of process routes P1 and P3 is around 0.35 kg CO_2-eq. per MJ, and thus significantly higher than the carbon footprints of P2 and P4 with about 0.30 kg CO_2-eq. per MJ. This is a result of the lower H_2 demand, including the anhydrous FA production. The environmental credit, *i.e.*, avoided burden, for CO_2 supply strongly reduces the carbon footprint of all process routes, especially P4 given that P4 requires 20% less H_2 per kg OME_{3-5} than P3. However, in P4, the environmental credit for CO_2 utilization is higher than that of P3, given that P4 requires 13% more CO_2 per kg of produced OME_{3-5} due to the lower C-selectivity towards OME_{3-5} in comparison to P3. For the carbon footprint of the electricity supply of 220 g CO_2-eq. per kW h_{el}, the PtX supply chain has a smaller carbon footprint than a fossil-based supply. If wind power is used for the electricity supply, the carbon footprint of the OME_{3-5} production is about −36 g CO_2-eq. per MJ, which is in good agreement with the literature results[10] for low-carbon future electricity supply. However, the current German power grid mix_{2018} is not suitable to improve the carbon footprint of the OME_{3-5} production, and thus high penetration of renewable energy generators is indeed for sustainable production.

Overall, routes P2 and P4 have the lowest carbon footprint independent of the carbon footprint of the electricity supply. Based on the sensitivity analysis with a future scenario for the German electricity mix, the carbon footprint of promising OME production routes such as P4 can reach 0.29 kg CO_2-eq. per l_{DE}, showing the opportunity for the sustainable production of OME. The TRL of the considered processes was evaluated in a conservative and optimistic manner at 3–7 based on experimental developments for critical process components of the OME value chain.

Considering the previous results, generally, there is no significant economic difference for the analysed OME production routes considered in this work. However, the overall energy efficiency of the considered processes shows a positive tendency for the anhydrous FA-based routes, which are still under research and development. An important lever to enhance the energy efficiency of the processes is to reduce the energy losses by valorising low temperature excess heat through usage in external processes. A big share of the excess heat (>43%) is still at useful temperature levels considering the usage of heat pump technology, an approach that is under investigation. This strategy is crucial in the context of PtX processes, where the production will probably take place where cheap renewable electricity is abundant. This will reduce the supply of external utility streams and besides the overall process efficiency enhacement, this can reflect positively on the NPC.

Given that the main driver of the production costs is the feedstock (H_2 and CO_2) with almost 74% of the NPC, the measures to create an economical frame for sustainable OME as neat fuel or a blend is significantly dependent on the H_2 production in areas with low levelized costs of electricity and with low costs for CO_2. The carbon footprint evaluation shows the potential of the environmental credit of OME production processes, which can reflect lower production costs when a WtW system boundary is considered. Monetary frames such as H_2 Global‡ from the federal German government and modifications in REDII§ on the European level to include

‡ H_2 Global is a funding concept by the federal German Government for short-term economic market entry into international PtX projects and achieving the goals adopted in the German National Hydrogen Strategy in connection with the production of green H_2 and its import.[91]

§ Renewable Energy Directive – Recast to 2030 (REDII) 2018/2001/EU.[92] In REDII, the overall EU target for renewable energy sources consumption by 2030 has been raised to 32%. Member states must ensure that a minimum of 14% of the final energy consumption in the transport sector is provided by fuel suppliers from renewable sources.

awarding systems and enhance the market introduction for sustainable fuels that lead to CO_2 avoidance are one of the main levers for the realization of the large-scale production of these fuels. The techno-economic and carbon footprint potentials of OME large-scale production processes in Germany and worldwide based on sensitivity analysis presented in this work emphasize the potential of OME as important constituents in a sustainable future mobility sector.

Abbreviations

ACC	Annual capital cost
AEL	Alkaline electrolysis
BEVs	Battery electrical vehicles
BMBF	German Federal Ministry of Education and Research
CAPEX	Capital expenditure
CCU	Carbon capture and utilization
CO	Carbon monoxide
CO_2	Carbon dioxide
COP	Coefficient of performance
CPS	Carbon from point sources
DAC	Direct air capture
DBU	German Federal Environmental Foundation
DME	Dimethyl ether
EC	Equipment cost
EGR	Exhaust gas recirculation
FA	Formaldehyde
FCI	Fixed capital investment
FfE	Research Centre for Energy Economics
Fuel	Active combustion substance
H_2	Hydrogen
H_2O	Water
HF	Poly(oxymethylene)hemiformals
ICEVs	Internal combustion engine vehicles
IEA	International Energy Agency
KPIs	Key performance indicators
LCA	Life cycle assessment
LCI	Life cycle inventory
LCIA	Life cycle impact assessment
LHV	Lower heating value
MEA	Mono-ethanol amine
MeOH	Methanol
MG	Poly(oxymethylene)glycols
NAMOSYN	Sustainable mobility through synthetic fuels
N_2	Nitrogen
NO_x	Nitrous oxides
NPC	Net production costs
O_2	Oxygen
OME_1	Methylal
OME_n	OME of chain length n
OMEs	Poly(oxymethylene)dimethyl ethers
OPEX	Operational expenditures
$OPEX_{dir/ind}$	Direct and indirect operational expenditures
$OPEX_{R\&U}$	Raw material and utility costs
PEM	Polymer electrolyte membrane
pFA	Paraformaldehyde
PtX	Power-to-X
RE	Renewable energy
SMR	Steam methane reforming
SOEC	Solid oxide electrolyser cell
TCI	Total capital investment
TEA	Techno-economic assessments
TEPET	Techno-economic process evaluation tool
TRI	Trioxane
TRL	Technology readiness level
UBA	German environment agency
VLLE	Vapor–liquid–liquid equilibria
WtW	Well-to-wheel

Symbols and indices

η	Efficiency
η_{mass}	Mass efficiency
η_C	Carbon efficiency
η_{energy}	Process energy efficiency
n	Order of the reaction
P	Pressure
T	Temperature
h_{labor}	Employee-hours per year
%	Percentage
l_{DE}	Litre diesel equivalent

Author contributions

Paper conception, the process modelling, simulation, the subsequent technical evaluation and workflow coordination was done by the Fraunhofer Institute for Solar Energy Systems ISE. KIT supported this work by evaluating the technological concepts and comparing it to the published state of the art. The cost estimation and subsequent economic evaluation was done by the DLR. The carbon footprint estimation and subsequent evaluation was done by the LTT of the RWTH Aachen University. TUM contributed to the conception, data analysis, critical revision for important content.

Conflicts of interest

The authors declare no competing financial interest.

Acknowledgements

The authors gratefully acknowledge funding by the German Federal Ministry of Education and Research (BMBF) within the NAMOSYN project "Sustainable mobility due to synthetic fuels". Franz Mantei also gratefully acknowledge the German Federal Environmental Foundation (DBU) for the funding provided for his Dissertation.[98,99]

References

1 German Environment Agency – Germany remains on track in climate protection "Deutschland bleibt im Klimaschutz auf Kurs", https://www.bundesregierung.de/breg-de/aktuelles/

klimaschutzziel-2020-erreicht-1876954, last accessed, June 2021.
2 European Parliament and of the Council, Regulation (EC) No. 715/2007 approval of motor vehicles with respect to emissions from light passenger and commercial vehicles (Euro 5 and Euro 6), http://eur-lex.europa.eu/legal-content/EN/ALL/?uri=CELEX:32007R0715, last accessed, August 2021.
3 Statistica Research Department – EU car sales: share of diesel engines 2015–2019, by country, https://www.statista.com/statistics/425113/eu-car-sales-share-of-diesel-engines-by-country/, last accessed, June 2021.
4 Statistica Research Department – EU car sales: share of diesel engines 2015–2019, by brand, https://www.statista.com/statistics/425324/eu-car-sales-share-of-diesel-engines-by-brand/, last accessed, June 2021.
5 International Energy Agency, *World Energy Outlook 2020, Outlook for Energy Demand*, https://www.iea.org/reports/world-energy-outlook-2020/outlook-for-energy-demand, last accessed, August 2021.
6 *Synthetic Fuels–OME$_1$: A Potentially Sustainable Diesel Fuel*, ed. E. Jacob and W. Maus, Wiener Motorensymposium, Vienna, 2014, 325–347, p. 35.
7 E. Jacob and W. Maus, *MTZ Worldw.*, 2017, **78**, 52.
8 M. Härtl, K. Gaukel, D. Pélerin and G. Wachtmeister, *MTZ Worldw.*, 2017, **78**, 52.
9 M. Münz, A. Mokros, D. Töpfer and C. Beidl, *MTZ Worldw.*, 2018, **79**, 16.
10 C. Hank, L. Lazar, F. Mantei, M. Ouda, R. J. White, T. Smolinka, A. Schaadt, C. Hebling and H.-M. Henning, *Sustain. Energy Fuels*, 2019, **3**, 3219.
11 H. Chen, R. Huang, H. Huang, M. Pan and W. Teng, *Appl. Therm. Eng.*, 2019, **150**, 591.
12 B. Lumpp, D. Rothe, C. Pastötter, R. Lämmermann and E. Jacob, *MTZ Worldw.*, 2011, **72**, 34.
13 H. Liu, Z. Wang, J. Wang, X. He, Y. Zheng, Q. Tang and J. Wang, *Energy*, 2015, **88**, 793.
14 S. E. Iannuzzi, C. Barro, K. Boulouchos and J. Burger, *Fuel*, 2017, **203**, 57.
15 J. Liu, H. Wang, Y. Li, Z. Zheng, Z. Xue, H. Shang and M. Yao, *Fuel*, 2016, **177**, 206.
16 J. Liu, P. Sun, H. Huang, J. Meng and X. Yao, *Appl. Energy*, 2017, **202**, 527.
17 A. Omari, B. Heuser, S. Pischinger and C. Rüdinger, *Appl. Energy*, 2019, **239**, 1242.
18 T. Popp, R. Lechner, M. Becker, M. Hebauer, N. O'Connell and M. Brautsch, *Appl. Therm. Eng.*, 2019, **153**, 483.
19 Y. R. Tan, M. L. Botero, Y. Sheng, J. A. Dreyer, R. Xu, W. Yang and M. Kraft, *Fuel*, 2018, **224**, 499.
20 J. Tian, Y. Cai, X. Pu, L. Gu, Y. Shi, Y. Cui and R. Fan, *Chem. Pap.*, 2018, **134**, 993.
21 Z. Wang, H. Liu, J. Zhang, J. Wang and S. Shuai, *Energy Procedia*, 2015, **75**, 2337.
22 H. Yang, X. Li, Y. Wang, M. Mu, X. Li and G. Kou, *Aerosol Air Qual. Res.*, 2016, **16**, 2560.
23 Y. Zhao, C. Geng, W. E, X. Li, P. Cheng and T. Niu, *Sci. Rep.*, 2021, **11**, 9514.
24 Y. Zhao, Y. Xie, X. Wang, Z. Li, T. Niu and S. Liu, *Energy Convers. Manag.*, 2020, **225**, 113489.
25 J. Preuß, K. Munch and I. Denbratt, *Fuel*, 2021, **303**, 121275.
26 D. Pélerin, K. Gaukel, M. Härtl, E. Jacob and G. Wachtmeister, *Fuel*, 2020, **259**, 116231.
27 P. Dworschak, V. Berger, M. Härtl and G. Wachtmeister, in *SAE Technical Paper Series*, SAE International, 400 Commonwealth Drive, Warrendale, PA, United States, 2020.
28 S. Deutz, D. Bongartz, B. Heuser, A. Kätelhön, L. S. Langenhorst, A. Omari, M. Walters, J. Klankermayer, W. Leitner, A. Mitsos, S. Pischinger and A. Bardow, *Energy Environ. Sci.*, 2018, **11**, 331.
29 M. Kass, M. Wissink, C. Janke, R. Connatser and S. Curran, in *SAE Technical Paper Series*, SAE International, 400 Commonwealth Drive, Warrendale, PA, United States, 2020.
30 M. Härtl and G. Wachtmeister, *Methanol Derived Synthetic Fuels for Diesel and Spark Ignited Engines, 4th Methanol Technology and Policy Commercial Congress*, Frankfurt am Main, 2017.
31 T. Wilharm and E. Jacob, *First Steps towards the Market Launch of OME Diesel*, 4th Methanol Technology and Policy Commercial Congress, Frankfurt an Main, 2017.
32 J. Perner and T. Steinfort, *Frontier Economics DER "Effizienzbegriff" in Der Klimapolitischen Debatte Zum S*, 2020.
33 C. J. Baranowski, A. M. Bahmanpour and O. Kröcher, *Appl. Catal., B*, 2017, **217**, 407.
34 D. N. D. Moulton, Diesel Fuel having improved qualities and method of forming, *US Pat.*, US5746785 A, 1998.
35 D. SanFilippo, R. Patrini and M. Marchionna, Use of an oxygenated product as a substitute of gas oil in diesel engines, *European Pat.* EP1422285A1, 2004.
36 K. D. Vertin, J. M. Ohi, D. W. Naegeli, K. H. Childress, G. P. Hagen, C. I. McCarthy, A. S. Cheng and R. W. Dibble, *Methylal and Methylal-Diesel Blended Fuels for Use in Compression-Ignition Engines*, 1999.
37 L. Lautenschütz, Neue Erkenntnisse in der Syntheseoptimierung Oligomerer Oxymethylendimethylether aus Dimethoxymethan und Trioxan, Inaugural dissertation, Ruprecht-Karls-Universität Heidelberg, 2015.
38 K. Hackbarth, P. Haltenort, U. Arnold and J. Sauer, *Chem. Ing. Tech.*, 2018, **90**, 1520.
39 J. Burger, E. Ströfer and H. Hasse, *Chem. Eng. Res. Des.*, 2013, **91**, 2648.
40 S. Schemme, J. L. Breuer, M. Köller, S. Meschede, F. Walman, R. C. Samsun, R. Peters and D. Stolten, *Int. J. Hydrogen Energy*, 2020, **45**, 5395.
41 D. Bongartz, J. Burre and A. Mitsos, *Ind. Eng. Chem. Res.*, 2019, **58**(12), 4881–4889.
42 M. Ouda, F. Mantei, K. Hesterwerth, E. Bargiacchi, H. Klein and R. J. White, *React. Chem. Eng.*, 2018, 676.
43 M. Held, Y. Tönges, D. Pélerin, M. Härtl, G. Wachtmeister and J. Burger, *Energy Environ. Sci.*, 2019, **12**, 1019.
44 C. J. Baranowski, M. Roger, A. M. Bahmanpour and O. Kröcher, *ChemSusChem*, 2019, **12**(19), 4421–4431.
45 N. Schmitz, J. Burger and H. Hasse, *Ind. Eng. Chem. Res.*, 2015, **54**, 12553.

46 N. Schmitz, E. Ströfer, J. Burger and H. Hasse, *Ind. Eng. Chem. Res.*, 2017, **56**, 11519.
47 N. Schmitz, C. F. Breitkreuz, E. Ströfer, J. Burger and H. Hasse, *Chemical Engineering and Processing – Process Intensification*, 2018, DOI: 10.1016/j.cep.2018.06.012.
48 N. Schmitz, C. F. Breitkreuz, E. Ströfer, J. Burger and H. Hasse, *J. Membr. Sci.*, 2018, **564**, 806.
49 D. Oestreich, L. Lautenschütz, U. Arnold and J. Sauer, *Chem. Eng. Sci.*, 2017, **163**, 92.
50 I. Hahnenstein, H. Hasse and G. Maurer, *Ind. Eng. Chem. Res.*, 1994, **33**, 1022–1029.
51 I. Hahnenstein, M. Albert, H. Hasse, C. G. Kreiter and G. Maurer, *Ind. Eng. Chem. Res.*, 1995, **34**, 440.
52 M. Maiwald, H. H. Fischer, M. Ott, R. Peschla, C. Kuhnert, C. G. Kreiter, G. Maurer and H. Hasse, *Ind. Eng. Chem. Res.*, 2003, **42**, 259.
53 M. Maiwald, T. Grützner, E. Ströfer and H. Hasse, *Anal. Bioanal. Chem.*, 2006, **385**, 910.
54 G. Maurer, *AIChE J.*, 1986, **32**, 932.
55 *Zukünftige Kraftstoffe*, ed. W. Maus, Springer Berlin Heidelberg, Berlin, Heidelberg, 2019.
56 F. Nestler, M. Krüger, J. Full, M. J. Hadrich, R. J. White and A. Schaadt, *Chem. Ing. Tech.*, 2018, **90**, 1409.
57 A. Otto, *Chemische, verfahrenstechnische und ökonomische Bewertung von Kohlendioxid als Rohstoff in der chemischen Industrie*, 2015.
58 D. Bongartz, L. Doré, K. Eichler, T. Grube, B. Heuser, L. E. Hombach, M. Robinius, S. Pischinger, D. Stolten, G. Walther and A. Mitsos, *Appl. Energy*, 2018, **231**, 757.
59 F. Nestler, A. R. Schütze, M. Ouda, M. J. Hadrich, A. Schaadt, S. Bajohr and T. Kolb, *Chem. Eng. J.*, 2020, **394**, 124881.
60 A. W. Franz, H. Kronemayer, D. Pfeiffer, R. D. Pilz, G. Reuss, W. Disteldorf, A. O. Gamer and A. Hilt, in *Ullmann's Encyclopedia of Industrial Chemistry*, Wiley-VCH Verlag GmbH & Co. KGaA, Weinheim, Germany, 2012.
61 S. Su, M. R. Prairie and A. Renken, *Appl. Catal., A*, 1993, **95**, 131.
62 J. Sauer and G. Emig, *Chem. Eng. Technol.*, 1995, **18**, 284.
63 J.-O. Drunsel, *Entwicklung von Verfahren zur Herstellung von Methylal und Ethylal*, Scientific Report Series, 2012.
64 R. W. Baker, *Membrane Technology and Applications*, J. Wiley, Chichester, New York, 2010.
65 M. S. Peters, K. D. Timmerhaus and R. E. West, *Plant Design and Economics for Chemical Engineers*, McGraw-Hill, Boston, 2003.
66 F. G. Albrecht, D. H. König, N. Baucks and R.-U. Dietrich, *Fuel*, 2017, **194**, 511.
67 S. Brynolf, M. Taljegard, M. Grahn and J. Hansson, *Renew. Sustain. Energy Rev.*, 2018, **81**, 1887.
68 J. Prause, M. Raab and R.-U. Dietrich, private communication, *Framework Assumptions TEA*, Begleitforschung Energiewende im Verkehr (BEniVer), 2020.
69 H. Naims, *Environ. Sci. Pollut. Res. Int.*, 2016, **23**, 22226.
70 K. Z. House, A. C. Baclig, M. Ranjan, E. A. van Nierop, J. Wilcox and H. J. Herzog, *Proc. Natl. Acad. Sci. U. S. A.*, 2011, **108**, 20428.
71 V. Bouillon-Delporte, J. Chatzimarkakis and N. Brahy, *Clean Hydrogen – Monitor 2020*, Hydrogen Europe Intelligence Departement, 2020.
72 R. Edwards, S. Godwin, H. Hamje, H. Hass, A. Krasenbrink, J.-F. Larivé, L. Lonza, H. Maas, R. Nelson, A. Reid, D. Rickeard, K. D. Rose and W. Weindorf, *Well-to-wheels Report Version 4.a: JEC Well-to-Wheels Analysis Well-to-Wheels Analysis of Future Automotive Fuels and Powertrains in the European Context*, Publications Office of the European Union, Luxembourg, 2014.
73 D. R. Woods, *Rules of Thumb in Engineering Practice*, Wiley-VCH, Weinheim, 2007.
74 *Ullmann's Encyclopedia of Industrial Chemistry*, Wiley-VCH Verlag GmbH & Co. KGaA, Weinheim, Germany, 2012.
75 M. E. Boot-Handford, J. C. Abanades, E. J. Anthony, M. J. Blunt, S. Brandani, N. Mac Dowell, J. R. Fernández, M.-C. Ferrari, R. Gross, J. P. Hallett, R. S. Haszeldine, P. Heptonstall, A. Lyngfelt, Z. Makuch, E. Mangano, R. T. J. Porter, M. Pourkashanian, G. T. Rochelle, N. Shah, J. G. Yao and P. S. Fennell, *Energy Environ. Sci.*, 2014, **7**, 130.
76 M. Fasihi, O. Efimova and C. Breyer, *J. Cleaner Prod.*, 2019, **224**, 957.
77 L. J. Müller, A. Kätelhön, S. Bringezu, S. McCoy, S. Suh, R. Edwards, V. Sick, S. Kaiser, R. Cuéllar-Franca, A. El Khamlichi, J. H. Lee, N. v. d. Assen and A. Bardow, *Energy Environ. Sci.*, 2020, **13**, 2979.
78 I. Kolakovic, H. Vreeswijk and F. Iscru, *Labour Costs in the EU, 60/2018*, Eurostat, Luxembourg, 2018.
79 International Organization for Standardization, *DIN EN ISO 14040: Environmental Management: Life Cycle Assessment: Principles and Framework*, 2006.
80 International Organization for Standardization, *DIN EN ISO 14044: Environmental Management: Life Cycle Assessment: Requirements and Guidelines*, 2006.
81 Forschungsstelle für Energiewirtschaft e.V. (FfE), *Ökobilanzen Synthetischer Kraftstoffe: Methodikleitfaden. 2020 [Research Center for Energy Economics (FfE), Life Cycle Assessments of Synthetic Fuels: Methodology Guide*, 2020.
82 G. Wernet, C. Bauer, B. Steubing, J. Reinhard, E. Moreno-Ruiz and B. Weidema, *Int. J. Life Cycle Assess.*, 2016, **21**, 1218.
83 *7th Energy Research Programme of the Federal Government – Research for an environmentally-friendly, reliable and affordable energy supply*, https://www.bmwi.de/Redaktion/EN/Artikel/Energy/research-for-an-ecological-reliable-and-affordable-power-supply.html, last accessed, June 2021.
84 H. Sperber, *Chem. Ing. Tech.*, 1969, **41**, 962.
85 F. Schorn, J. L. Breuer, R. C. Samsun, T. Schnorbus, B. Heuser, R. Peters and D. Stolten, *Advances in Applied Energy*, 2021, **3**, 100050.
86 A. Zimmermann, R. Schomäcker, E. Gençer, F. O'Sullivan, K. Armstrong, P. Styring and S. Michailos, *Global CO_2 Initiative Complete Oxymethylene Ethers Study 2018*, 2019.
87 A. O. Oyedun, A. Kumar, D. Oestreich, U. Arnold and J. Sauer, *Biofuels, Bioprod. Biorefin.*, 2018, **89**, 3315.
88 M. Martín, J. Redondo and I. E. Grossmann, *ACS Sustainable Chem. Eng.*, 2020, **8**, 6496.

89 N. Schmitz, J. Burger, E. Ströfer and H. Hasse, *Fuel*, 2016, **185**, 67.
90 S. Deutz and A. Bardow, *Nat. Energy*, 2021, **6**, 203.
91 *FReSMe Project – From Residual Steel Gases to Methanol*, https://www.carbonrecycling.is/news-media/fresme-project-reaches-final-milestone-from-blast-furnace-waste-emissions-to-ferry-fuel, last accessed, August 2021.
92 K. Roh, A. Bardow, D. Bongartz, J. Burre, W. Chung, S. Deutz, D. Han, M. Heßelmann, Y. Kohlhaas, A. König, J. S. Lee, R. Meys, S. Völker, M. Wessling, J. H. Lee and A. Mitsos, *Green Chem.*, 2020, **22**, 3842.
93 S. Su, P. Zaza and A. Renken, *Chem. Eng. Technol.*, 1994, **17**, 34.
94 J.-O. Weidert, J. Burger, M. Renner, S. Blagov and H. Hasse, *Ind. Eng. Chem. Res.*, 2017, **56**, 575.
95 *Prefere paraform, products, Dimethoxymethane (Methylal)*, Prefere Resins Holding GmbH, https://prefere.com/de/paraform/produkte/dimethoxymethan, last accessed, August 2021.
96 N. Suratman, *INEOS Paraform starts up new methylal plant in Germany*, Independent Commodity Intelligence Services, 2012, https://www.icis.com/explore/resources/news/2012/08/07/9584533/ineos-paraform-starts-up-new-methylal-plant-in-germany/, last accessed, August 2021.
97 A. Ferre, J. Voggenreiter, Y. Tönges and J. Burger, *MTZ Worldw.*, 2021, **82**, 26.
98 *Hydrogen Energy Partnerships for Climate protection and industrial growth*, https://h2-global.de/, last accessed, 21.07.16.
99 European Commission, *Promotion of the Use of Energy from Renewable Sources: 2018/2001/EU: REDII: 2018/2001/EU*, 2018.